N84-27024

Progress Report

Experimental Study Using Nearfield Acoustical Holography of Sound Transmission through Fuselage Sidewall Structures

NASA Grant NAG 1-216

J. D. Maynard
Department of Physics
The Pennsylvania State University
University Park, PA 16802

This report describes the work accomplished in the project "Experimental Study Using Nearfield Acoustical Holography of Sound Transmission through Fuselage Sidewall Structures" (NASA grant NAG 1-216) beginning October 15, 1983. Briefly, the project involves the development of the Nearfield Acoustic Holography (NAH) technique (in particular its extension from single frequency to wideband noise measurement) and its application in a detailed study of the noise radiation characteristics of several samples of aircraft sidewall panels. With the extensive amount of information provided by the NAH technique, the properties of the sound field radiated by the panels may be correlated with their structure, mounting, and excitation (single frequency or wideband, spatially correlated or uncorrelated, structure-borne or air-borne).

As discussed in the renewal proposal of August 1983, the work accomplished at the beginning of this grant period included:

1) Calibration of the 256 microphone array and test of its accuracy.
2) Extension of the facility to permit measurements on wideband noise sources. The extensions included the addition of high-speed data acquisition hardware and an array processor, and the development of new software.
3) Installation of motion picture graphics for correlating panel motion with structure, mounting, radiation, etc.
4) Development of new holographic data processing techniques.

A summary of the effort expended since the beginning of the current grant period is presented below:

1. Publications and presentations.

Considerable time was spent in the preparation of papers and talks describing the new features (listed above) of the NAH technique and its applications. A list of the papers, etc. (not including colloquia and seminars) is as follows:

a) A plenary session talk was presented at the 106th meeting of the Acoustical Society of America in San Diego (November 1983). The title was "Nearfield Acoustical Holographic Techniques Used to Visualize Radiated Sound Fields."

b) A paper providing a general review of the NAH technique in theory, development, and application has been submitted to J. Acoust. Soc. Am. The title is "Nearfield Acoustic Holography (NAH): I. Theory of Generalized Holography and the Development of NAH." This paper reviews much of our progress relevant to this grant; rather than repeat the discussion of the technical accomplishments here, a preprint of the paper is presented in Appendix I.

c) A technical paper presenting the details of the NAH holographic reconstruction algorithms has been prepared for J. Acoust. Soc. Am. The title is "Nearfield Acoustic Holography (NAH): II. Computer Algorithms." A preprint of this paper will be forwarded in the near future, pending editorial corrections.

d) A master's thesis entitled "Test of the Nearfield Acoustical Holography Technique Using an Unbaffled Uniformly Oscillating Disk" has been completed by Todd Beyer. A paper will be prepared from this thesis.

e) Six talks were presented by the graduate students and research associate working on the NAH project at the 107th meeting of the American Acoustic Society in Norfolk (May 1984). The titles of these talks were:

The Implementation of Nearfield Acoustic Holography with an Array Processor.

Experimental Studies of Acoustic Radiation for Unbaffled Complex Planar Sources with Nearfield Acoustic Holography.

Advances in Nearfield Acoustical Holography (NAH) Algorithms I. Green's Functions.

Advances in Nearfield Acoustical Holography (NAH) Algorithms II. Zoom Imaging.

Holographic Reconstruction of Odd-shaped 3-D Sources.

Nearfield Holography for Wideband Sources.

For further details on this work, see the abstracts in Appendix II.

2. Controlled noise synthesizer.

In order to begin controlled studies of noise sources, it was necessary to construct a noise synthesizer to produce well characterized types of noise. As discussed in the original proposal, we wish to be able to vary both the temporal and spatial coherence of the forces driving a panel in order to observe how coherence effects the radiated sound field, in particular we wish to see how both types of coherence effect circulating energy flow patterns (which always occur with single frequency point excitation) and radiation efficiency.

Graduate student Donald Bowen has constructed an electronics unit which contains a computer and clock interface and four identical channels consisting of read/write memory, digital-to-analog (D/A) converters, and filters. Through the computer interface, number sequences having a preselected coherence are loaded into the memories of the four channels. The clock interface is connected to the data acquisition clock of the NAH array so that readout of the noise sequence through the D/A converters to the drivers (as many as four, spatially

distributed) exciting the panel(s) is synchronized with the hologram recording. An extra advantage of using this separate noise synthesizer (rather than using the computer's D/A directly) is that the computer is free to perform the reconstructions of the previous hologram, while the current hologram recording occurs off-line.

It should be noted that this device is ideally suited for determining the most efficient method for active cancellation of panel radiation; both the panel excitation (possibly wideband) and the cancellation signal may be preselected in order to permit a controlled study of the radiated field.

3. Measurements with structure-borne excitation.

Upon completion of the new data acquisition system and programing of the new array processor, a program of measurements on several samples of ribbed panels was initiated. The panels were point excited at a number of resonance frequencies, and vibration patterns, maps of the acoustic vector intensity field, and radiation efficiencies were obtained in each case. Research Associate Yongchun Lee, whose Ph.D. research was in structure vibration, wrote a computer program for modeling the vibration and radiation from simulated ribbed panels. The computer modeling is now being used to search for systematic behavior in the correlation between the properties of the panel and the properties of the radiated sound field. The results of this work were reported at the Norfolk ASA meeting (see relevant abstract in Appendix II).

4. Air-borne sound excitation facility.

One of the major tasks of the original proposal was to compare the radiated sound fields between panels driven with structure-borne sound and with air-borne sound. When making measurements while driving with air-borne sound, it is of course necessary to isolate the driving field from the re-radiated (transmitted) field, as in a conventional transmission loss measurement. Usually such measurements are made with two rooms separated by a massive wall

containing the test panel. Rather than try to transport our holographic array to such a facility, we decided to construct a less elaborate device, based on one used to test aircraft panels at NASA Langley. This device, shown in the attached figure, uses the sound pressure in a relatively small, carefully sealed chamber to drive the aircraft panel. The sound pressure in the chamber is driven by nine loudspeakers in the wall of the chamber. The sound from the backside of the speakers is prevented from diffracting into the radiated field of the panel by nine sealed boxes, packed with fibreglass wool, enclosing the backs of the speakers.

Nearfield holographic measurements of the samples of aircraft panels driven with airborne sound are now in progress. Tests of the panels driven with structure-borne sound will be repeated with the panels mounted in the new device, since the boundary conditions at the edges of the panels will be different from the earlier measurements with free-edge conditions. Once all the holographic reconstructions are complete, they will be examined for systematic features relating panel structure, mounting, and excitation to the radiated sound field.

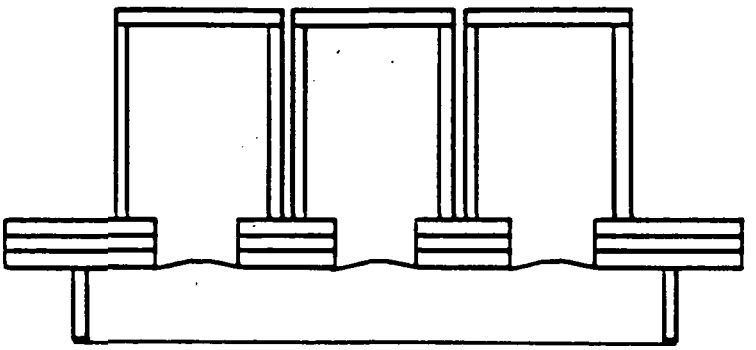

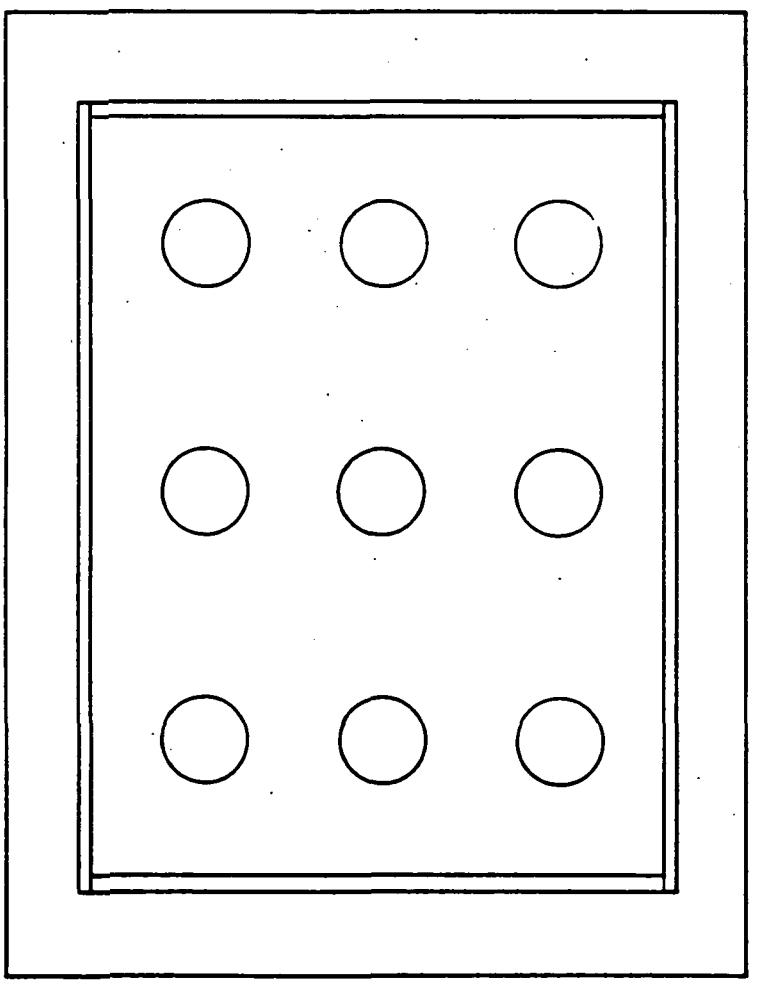

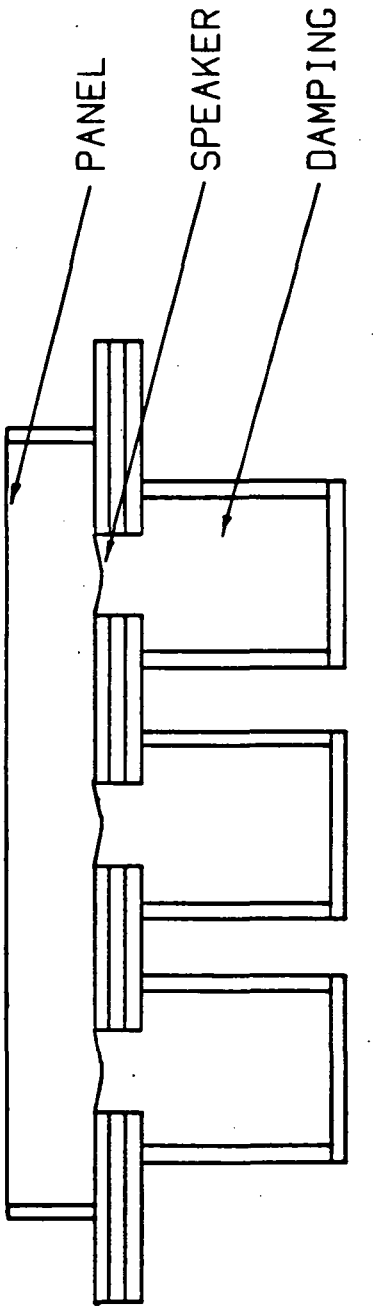
PANEL
SPEAKER
DAMPING

APPENDIX I

Nearfield Acoustic Holography (NAH)

I. Theory of Generalized Holography and the Develoment of NAH

J. D. Maynard, E. G. Williams,* and Y. Lee

The Pennsylvania State University

Department of Physics

University Park, PA 16802

Because its underlying principles are so fundamental, holography has been studied and applied in many areas of science. Recently a technique has been developed which takes the maximum advantage of the fundamental principles and extracts much more information from a hologram than is customarily associated with such a measurement. In this paper the fundamental principles of holography are reviewed, and a sound radiation measurement system, called Nearfield Acoustic Holography, which fully exploits the fundamental principles, is described.

*Present address: Naval Research Lab.

TABLE OF CONTENTS

I. INTRODUCTION

Since the time of its conception around 1950, holography[1] has become an increasingly powerful research tool. However, in conventional optical and acoustical holography the full potential of the technique has not been realized. In acoustical holography one can obtain much more information from a hologram than is customarily associated with such a measurement. In this paper we outline the fundamental theory and experimental and signal processing requirements for what we refer to as "generalized holography" which fully exploits the potential of the technique. We also describe the practical application of generalized holography in an actual experimental measurement system called Nearfield Acoustical Holography (NAH).

On a fundamental level, the great utility of holography arises from its high information content; that is, data recorded on a two-dimensional surface (the hologram) may be used to reconstruct an entire three-dimensional wavefield, with the well-known result of obtaining three dimensional images. A popular science magazine once noted that if a picture is worth a thousand words, then a hologram is worth one-thousand to the three-halves power, or approximtely 32,000 words. In the case of digitally processed holograms this statement is literally correct; if a sampled two-dimensional hologram contains 1000 digital words of data, and if the reconstruction is performed for a cubical three-dimensional region, then the resulting reconstruction will contain $1000^{3/2}$ digital words of data. An actual digitally-sampled hologram may contain hundreds of thousands of words of data, and the amount of reconstruction data is limited only by the restriction of computation time. In generalized holography, the reconstruction may be expanded in other ways as well. For example, in Nearfield Acoustic Holography, the recording of the sound pressure field on a two-dimensional surface can be used to determine not only the three-dimensional sound pressure field but also the particle velocity field, the acoustic vector intensity field, the surface

velocity and intensity of a vibrating source, etc. Furthermore each data point in the hologram need not be simply phase information from single frequency radiation, but may be a complete time sequence recording from incoherent "white-light" or noise radiation; in this case one may not only reconstruct a three-dimensional field, but may also observe its evolution in time. An interesting application would be the visualization of energy flow from a transient source. Generalized holography also removes the generally assumed limitations of conventional holography, such as the resolution of a reconstructed image being limited by the wavelength of the radiation[2-6] and the limited field of view resulting from conventional recording requirements.

II. EXAMPLE OF APPLICATION

Before describing the theory and implementation of generalized holography, it would be worthwhile to motivate its development by discussing a fundamental research area in acoustics which dramatically illustrates the utility of the technique.[7] This research area is the study of the radiation of sound into a medium, such as air or water, by a complex vibrator. The basic objective in this area is to correlate properties of the vibrator [such as structural features, modes of vibration, implementation of quieting techniques, etc.] with properties of the radiated sound field [such as the total power radiated, the farfield radiation pattern, the vector intensity field, etc.]. From the standpoint of acoustic fundamentals, this is a very difficult problem even in the simplest cases. For example: although the sound field of a plane, rectangular vibrator in an infinite rigid baffle is easily calculated, the sound field of such a vibrator in free space, without the baffle, is impossible to determine analytically and can only be approximated with formidable calculations on a large computer. If the vibrator is made more complex with the addition of ribs, etc., the precise calculations become more difficult, and we are left with little on which to establish an understanding of how the vibrator couples acoustic energy into the medium.

Correlating vibrator features with sound field properties is a difficult problem also from the standpoint of acoustic measurement. Consider for example the simple case of a rectangular plate vibrating in a normal mode with some definite nodal line pattern. The plate may have some nominal displacement amplitude producing some nominal particle velocity amplitude v_o and pressure amplitude P_o in the medium around the plate. If the plate is below coincidence[8] [with the acoustic wavelength in the medium larger than the typical plate dimension], then relatively little acoustic energy will be radiated into the farfield. However,

another plate, also producing a similar velocity amplitude v_o and pressure P_o may be above coincidence and subsequently radiate a relatively large amount of acoustic energy into the farfield. The point here is that a measurement of only vibrator displacements, particle velocity, or sound pressure around a vibrator is not sufficient to determine how the vibrator delivers energy into the sound field. At high frequencies, well above coincidence, there is not much problem because areas of the vibrator which have large displacements are probably the major energy producing sources. However, many sound sources such as rotating machinery, musical instruments, etc. radiate at low frequencies such that the radiated wavelengths are larger than the typical dimensions of the vibrator's features. In this case, areas of large displacements or large pressure amplitudes are not necessarily energy sources and may in fact be large sinks of acoustic energy.

The quantity which is necessary for determing how a vibrator radiates sound is the acoustic intensity vector field $\vec{S}(\vec{r})$, which (for radiation at a single frequency) is given by the product of the pressure amplitude, the velocity amplitude, and the cosine of the phase between them:[9] $\vec{S}(\vec{r}) = \frac{1}{2} P_o(\vec{r}) \vec{v}_o(\vec{r}) \cos \theta$. As a vector field, it gives, at each point in space, the rate and direction of acoustic energy flow. At points on a vibrator where the normal component of this field is large, the location of a valid energy source may be assumed. Because of this property of the intensity field there has been much interest in its measurement, and methods such as the "two-microphone" technique[10] have been developed. However, such techniques are limited because they measure the vector intensity [actually only one component of it] at a single point in space, or in an average over some region in space. With such limited data one may mistakenly identify an area as a radiating source when it may in fact be a part of a circulating energy flow pattern.[7] That is, energy may leave a part of a

vibrator only to quickly [within a wavelength] turn around and flow back into another part of the vibrator, subsequently being returned through the vibrator back to the "source" area. Such a circulation represents real energy flow and not a reactive type of energy as would be represented by the product of the out-of-phase parts of the pressure and particle velocity fields. In order to measure with confidence the sound energy radiation from a complex vibrator it is necessary to obtain a detailed map of the energy flow field so as to correctly identify possible circulating flow patterns. Mapping the vector intensity field at tens-of-thousands of points in space with a point-by-point probe is impractical; however, with Nearfield Acoustic Holography such information is readily obtained. As will be discussed in more detail later, the features of the actual NAH system are:

1) The technique involves only a single, non-contact measurement. The system uses an open array of microphones positioned uniformly over a two-dimensional surface.

2) It is a high-speed technique. With our prototype system we can put a test source under the microphone array and produce displays of its sound radiation within a matter of minutes. Such a fast turn-around time permits the researcher to spend more time studying the vibrator/radiation relationship rather than making tedious measurements.

3) The measurement covers a large area. With our prototype system we can pinpoint acoustic energy sources within an area of nearly 10 m^2.

4) The measurement area subtends a large solid angle from the sources. This means that multidirectional sources can be measured without missing information.

5) The technique has high spatial resolution; our prototype system can pinpoint energy sources to within ~5 cm.

6) The output of the technique can be computer graphic displays of:

a) The sound pressure field, from source to farfield.

b) The particle velocity field, from source to far field.

c) Modal structure of a vibrating surface (determined from the normal particle velocity evaluated at the surface).

d) The vector intensity field, which can be used to locate the energy producing sources and to map the energy flow throughout the sound field.

e) The farfield radiation pattern.

f) The total power radiated.

For either single frequency, transient, or wideband noise sources, the fields a) - e) listed above may be observed to evolve in real time through the use of motion picture computer graphics. With such a complete set of visualized information, one may more readily gain insight into the salient fetaures (effects of fluid loading, for example) of the otherwise obscure interaction between a complex vibrating structure and the acoustic medium. How generalized holography permits so much information to be obtained efficiently is discussed in the following section.

III. CONVENTIONAL AND GENERALIZED HOLOGRAPHY

In holography, localized sources, which may be scattering (or diffracting) objects or active sources, produce a unique wavefield in a three-dimensional region. Measurements of the wavefield are made on a two-dimensional surface, usually a plane surface (the hologram plane), and this data is used to reconstruct the wavefield throughout the three-dimensional region; large amplitudes in the reconstruction provide an image of the source object. That the data on the two-dimensional surface is sufficient to reconstruct the three-dimensional field is due to the fact that the field obeys the wave equation, and a known Green's function (as will be discussed subsequently) can be used. It is worth noting that in acoustics, holography is the only measurement technique which takes full advantage of the simple but powerful fact that the field being measured obeys the wave equation.

The description of holography in the paragraph above provides a basic definition of generalized holography, and it might seem to be an appropriate description of conventional holography as well. However, whereas the notions of generalized holography are comprehensive and exact, conventional holography has significant restrictions and limitations. In most applications of conventional holography:

1) The hologram is recorded with monochromatic (single frequency) radiation only. The conventional technique is not usually applied to incoherent white-light or noise sources.

2) The hologram is recorded with a reference wave and primarily phase information only is retained with a "square-law" detector.

3) The spatial resolution of the reconstructed image is limited by the wavelength of the radiation;[2-6] that is, two point sources cannot be resolved if they are closer together than about one wavelength. In optical holography this

is not a serious limitation since the optical wavelengths are so small. In acoustics, however, the radiated wavelengths may be considerably larger than the typical dimensions of the source features, and in this case it would be impossible to pinpoint those features which might be relevant to the energy radiation. Thus conventional acoustical holography must be rejected as a means of studying a large class of long wavelength radiators such as vibrating machinery, musical instruments, etc.

4) If the hologram records a particular scalar field, then only this scalar field can be reconstructed. Thus in acoustical holography, if the sound pressure field is recorded, then one cannot reconstruct an independent particle velocity field or the vector intensity field, and one cannot image the true energy producing sources or map the flow of acoustic energy. The dramatic advantages of the technique described in the preceding section are not present in conventional holography.

5) In order for the conventional holographic reconstruction process to work, the hologram must be recorded in the Fresnel or Fraunhofer zone of the wavefield (i.e., many wavelengths from the source).[11] Because of the practical limitation of finite hologram size, the hologram may subtend a small solid angle from the source. If the source is directional, some important information may be missed by the hologram.

If the causes of the above limitations are examined, it is found that they are not intrinsic to the fundamental theory of holography, but rather are due to experimental limitations which are always present in optical holography, but are not necessarily present in acoustical holography. In the past, the techniques of acoustical holography were adopted from the technology of optical holography, and methods of removing the limitations in long-wavelength acoustical holography were not pursued.

IV. FUNDAMENTALS OF GENERALIZED HOLOGRAPHY

A. General

As discussed in the preceding sections, generalized holography involves the measurement of a wavefield on an appropriate surface and the use of this measurement to uniquely determine the wavefield within a three-dimensional region. This description indicates that generalized holography is equivalent to the use of a Dirichlet boundary condition[12] on a surface for which the Green's function is known. One usually imagines boundary value problems as having boundary conditions determined by a source (for example, a vibrating surface in an acoustics problem); such problems are difficult because the source may provide conditions for which there is no known Green's function. In generalized holography, one simply measures a uniform (Dirichlet or Newman) boundary condition on a surface for which there is a known Green's function. The holographic reconstruction process is then simply the convolution (or deconvolution) of the measured boundary values with the Green's function. In theory this is a straightforward process; in practice some care must be taken in order to identify and avoid the limitations of conventional holography. The causes of the limitations occur in the method of measuring the boundary data, in the formulation of the Green's function, and in the evaluation of the convolution integral. These areas will be discussed in subsequent sections. In later sections the calculation of quantities other than the measured wavefield will be discussed. We begin with a description of the formal assumptions required for generalized holography.

The basic assumption is that some sources are creating a wavefield $\psi(\vec{r},t)$ [a function of position $\vec{r}$ in a three-dimensional region of space and time t] which, within a three-dimensional region of interest, satisfies the homogeneous wave equation

$$\nabla^2\psi = \frac{1}{C^2}\frac{\partial^2\psi}{\partial t^2} \tag{1}$$

Here ^{2} is the Laplacian operator and C is a constant propagation speed. It is further assumed that:

1) There is a surface S enclosing the three-dimensional region of interest for which there is a known Green's function $G(r|r_S)$ satisfying the homogeneous Helmholz equation for $\vec{r}$ inside S and vanishing [or having a vanishing normal derivative] for $\vec{r} = \vec{r}_S$ on S. Part of S may be at infinity; in practice the part of S not at infinity will be a level surface of some separable coordinate system which is in close contact with the sources.

2) There is a surface H (the hologram surface) which may coincide with S or have a level surface parallel to S for which $\psi(\vec{r}_H,t)$ [or its normal derivative] can be measured or assumed for all $\vec{r}_H$ on H and all t.

If the above conditions are met, then $\psi(\vec{r},t)$ for $\vec{r}$ inside S can be uniquely determined from $\psi(\vec{r}_H,t)$ with $\vec{r}_H$ on H. The exact procedure and a discussion of the consequences resulting from deviations from the assumptions are presented in the following subsections.

B. Time dependence

The first step in finding $\psi(\vec{r},t)$ from $\psi(\vec{r}_H,t)$ is to Fourier transform in time:

$$\tilde{\psi}(\vec{r},\omega) = \int_{-\infty}^{\infty} \psi(\vec{r},t)e^{i\omega t}\,dt \tag{2}$$

and

$$\tilde{\psi}(\vec{r}_H,\omega) = \int_{-\infty}^{\infty} \psi(\vec{r}_H,t)e^{i\omega t}\,dt \quad . \tag{3}$$

The symbol ~ indicates a complex field having an amplitude and phase depending on $\vec{r}$. The wave equation becomes the Helmholz equation

$$\nabla^2\tilde{\psi}(\vec{r},\omega) + k^2\tilde{\psi}(\vec{r},\omega) = 0 \tag{4}$$

with wavenumber $k = \omega/c$. It should be noted that formally the boundary data (r_S,t) must be measured for all time $-\infty \leq t \leq \infty$. $\psi(\vec{r}_S,t)$ may be measured within a finite time window of duration T if $\psi(\vec{r}_S,t)$ is known to be periodic with period T. For a noise source, one may assume that there exists a time scale T for which statistical averages become stationary within specified limits of fluctuation;[13] in this case also a finite Fourier transform is sufficient. For most noise sources a reasonable T can be used; however there are exceptions where T may be so large as to preclude the acquisition of a manageable amount of data. An example would be a high frequency transient in a highly reverberant room. In digital holography, $\psi(\vec{r}_H,t)$ is sampled at N discrete points in time $t_n = t_{\vec{r}_H} + nT/N$ (noting that the starting time $t_{\vec{r}_H}$ may be different for different positions on the surface H). It is assumed that the sampling is accomplished at the Nyquist rate to prevent aliasing in the time domain. Expression (3) becomes

$$\tilde{\psi}(\vec{r}_H,\omega_m) \approx e^{i\omega_m t_{\vec{r}_H}} \left[\sum_{n=0}^{N-1} \psi(\vec{r}_H,t_n) e^{i2\pi nm/N}\right] \frac{T}{N} \qquad (5)$$

with $\omega_m = 2\pi m/T$ and m is a non-negative integer less than N/2. The summation in brackets can now be accomplished with a fast-Fourier-transform (FFT) computer algorithm. The errors associated with the approximation (5) are not unique to holography but are common to all signal processing involving discrete, finite-window sampling. Since discussions of these errors can be found in any text on signal processing,[14] we shall not concern ourselves with them here; the more interesting aspects of generalized holography are found in the spatial, rather than the temporal, signal processing. For the purpose of the spatial analysis in the next sections, it can be assumed that the sources are driven at frequencies $\omega_m = 2\pi m/T$ with $m(< N/2)$ some integer and T and N

fixed. For most sources it can be assumed that the wavefield generated by these harmonic sources doesn't differ significantly from the actual wavefield. If the actual operating frequency of the source is known, then signal processing techniques can be used to correct $\tilde{\psi}(\vec{r}_H,\omega_m)$. At any rate, for sources operating at the set of frequencies ω_m, expression (5) becomes exact.

For the spatial analysis we consider a fixed value of ω so that there is a fixed wavenumber $k = \omega/c$ and a single characteristic wavelength $\lambda = 2\pi c/\omega$. The spatial problem is now to find the complex field $\tilde{\psi}(\vec{r})$ satisfying the homogeneous Helmholz equation

$$\nabla^2\tilde{\psi}(\vec{r}) + k^2\tilde{\psi}(\vec{r}) = 0 \tag{6}$$

for $\vec{r}$ within the three-dimensional region of interest, given $\tilde{\psi}(\vec{r}_H)$ for $\vec{r}_H$ on the hologram surface H.

At this point the source of one of the limitations of optical holography can be discussed. In order to carry out the spatial processing it is necessary to use the complex field $\tilde{\psi}(\vec{r}_H)$, amplitude as well as phase, for each temporal frequency. In theory $\psi(\vec{r}_H)$ can be found from $\psi(\vec{r}_H,t)$; however, in optics there is no detector fast enough to record the real time development of the wavefield. Instead the recorded wavefield must contain only a single temporal frequency, the source wavefield must be mixed with a reference wave, and the resultant is recorded with a square-law detector.[11] The contributions to this (zero-frequency) recording which come from the cross-terms in the mixed wavefield can be used to obtain some information about $\tilde{\psi}(\vec{r}_H)$; however the amplitude and phase information have become irretrievably intermixed. In practice, optical holograms are measured many wavelengths from the source (in the Fresnel or Fraunhofer zone) where the amplitude information has become unimportant (having a simple spherical wave dependence on distance from the source) and only the phase information is significant. The phase information contained in the optical

hologram cross-terms can be processed as $\tilde{\psi}(\vec{r}_H)$; however the lack of precise amplitude and phase information and the requirement of recording in the Fresnel or Fraunhofer zone results in the limitations of conventional optical holography as described in Section II. These limitations will be discussed further in a later subsection. For generalized holography it is assumed that $\psi(\vec{r}_H)$ is known.

In acoustical holography it is possible to record $\psi(\vec{r}_H,t)$ with conventional experimental techniques and precisely determine $\tilde{\psi}(\vec{r}_H)$. It is interesting to note that early implementations of acoustical holography were copies of optical systems in that reference waves were used and square-law recordings were made in the farfield of the source.[15]

C. Spatial processing

Since it is assumed that the Green's function $G(\vec{r}|\vec{r}_S)$ satisfying the homogeneous Dirichlet condition on the surface S is known, then the solution $\tilde{\psi}(\vec{r})$ for Equation (6) can be found with a surface integration:[12]

$$\tilde{\psi}(\vec{r}) = -\frac{1}{4\pi}\iint \tilde{\psi}(\vec{r}_S)\,\frac{\partial G}{\partial n}\,(\vec{r}|\vec{r}_S)\,d^2r_S \qquad (7)$$

where $\partial G/\partial n$ is the normal derivative of G with respect to $\vec{r}_S$. If the surface S is the same as the surface H where $\tilde{\psi}(\vec{r}_H)$ is measured or assumed then the determination of $\tilde{\psi}(\vec{r})$ is complete. If H lies inside S then processing proceeds as follows:

In practice, the Green's function G is known provided that the part of S not at infinity is the level surface of a separable coordinate system. We denote the three spatial coordinates of this system as ξ_1, ξ_2, and ξ_3, with the level surface given by $\xi_3 = \xi_3^S$, a constant. According to the assumptions of generalized holography (in Section II) the hologram surface is given by $\xi_3 = \xi_3^H$, where the constant $\xi_3^H > \xi_3^S$ describes a surface inside S. In terms of ξ_1, ξ_2, and ξ_3 Equation (7) becomes

$$\tilde{\psi}(\xi_1,\xi_2,\xi_3) = -\frac{1}{4\pi}\iint \tilde{\psi}(\xi_1'\xi_2'\xi_3^S)\left[\frac{\partial G}{\partial \eta}(\xi_1-\xi_1', \xi_2-\xi_2', \eta)\Big|_{\eta=\xi_3-\xi_3'}\right] d\xi_1' d\xi_2' \quad (8)$$

but this cannot be evaluated directly because $\tilde{\psi}(\xi_1,\xi_2,\xi_3^H)$ known instead of $\tilde{\psi}(\xi_1,\xi_2,\xi_3^S)$. If expression (8) is evaluated for $\xi_3 = \xi_3^H$ we obtain

$$\tilde{\psi}(\xi_1,\xi_2,\xi_3^H) = \iint \tilde{\psi}(\xi_1',\xi_2',\xi_3^S) G_{HS}(\xi_1-\xi_1', \xi_2-\xi_2') d\xi_1 d\xi_2 \quad (9)$$

where $G_{HS}(\alpha,\beta) = (-1/4\pi)\partial G/\partial\eta(\alpha,\beta,\eta)|_{\eta=\xi_3^H-\xi_3^S}$. The right-hand-side of Equation (9) is a two-dimensional convolution; by using the convolution theorem Equation (9) can be inverted to obtain $\tilde{\psi}(\xi_1,\xi_2,\xi_3^S)$ in terms of $\tilde{\psi}(\xi_1,\xi_2,\xi_3^H)$. Denoting a two-dimensional spatial Fourier transform by $\hat{}$ and its inverse by F^{-1}, we have from Equation (9) and the convolution theorem:

$$\hat{\tilde{\psi}}(\xi_3^H) = \hat{\tilde{\psi}}(\xi_3^S)\cdot\hat{G}_{HS} \quad . \quad (10)$$

Solving for $\tilde{\psi}(\xi_1,\xi_2,\xi_3^S)$ yields:

$$\tilde{\psi}(\xi_1\xi_2\xi_3^S) = F^{-1}\left[\hat{\tilde{\psi}}(\xi_3^H)\cdot\hat{G}_{HS}^{-1}\right] \quad (11)$$

Once $\tilde{\psi}(\xi_1,\xi_2,\xi_3^S)$ is found from the hologram data $\tilde{\psi}(\xi_1,\xi_2,\xi_3^H)$, then equation (8) is used to reconstruct $\tilde{\psi}(\xi_1,\xi_2,\xi_3)$ over the entire three-dimensional region inside S. It should be noted that the two-dimensional Fourier transforms used in Equations (10) and (11) may be in the form of decompositions in terms of a complete set of eigenfunctions appropriate for the coordinate system used. In fact, the Green's function is usually only known in terms of such a decomposition. This feature will become evident in subsequent subsections.

If instead of $\tilde{\psi}(\vec{r}_S)$ one determines its normal derivative with respect to $\vec{r}_S$, $\partial\psi/\partial n(\vec{r}_S)$, then Equation (7) is replaced by[12]

$$\tilde{\psi}(\vec{r}) = +\frac{1}{4\pi}\iint \frac{\partial\psi}{\partial n}(\vec{r}_S) G(\vec{r}|\vec{r}_S) d^2 r_S \quad (12)$$

where the Green's function G now must satisfy a homogeneous Neuman condition on S. Processing in terms of a separable coordinate system proceeds as before.

Derivatives of the field $\psi(\vec{r})$ with respect to the three spatial coordinates may be transferred to the Green's functions in Equations (7) and (12), so that calculations of such quantities simply involve processing with a different kernel.

It is important to note that all of the formulations discussed above [Equations (7)-(12)] are exact; there have been no approximations which would lead to resolution limits, etc. Equations (7) and (12) are not approximate expressions of Green's theorem nor are they approximate solutions to the Helmholz integral equation; they should not be confused with the approximate formulas used in diffraction problems.[2] The Green's functions in Equations (7) and (12) should not be confused with the free-space Green's function even though in some cases it has an identical form. Historically Equations (7) and (12) are referred to as the first and second Rayleigh integrals.[16]

D. Plane generalized holography

In conventional holography, holograms are usually recorded on plane surfaces, and in generalized holography the processing of plane holograms is the easiest from a computational point of view. Other hologram surfaces (cylindrical, spherical, etc.) can be used when they more closely conform to the shape of the sources. When the sources have odd shapes which do not conform to the level surface of a separable coordinate system, then plane generalized holography may use in conjunction with a finite-element technique; this will be discussed in the section of Further Developments. In any case the features of plane generalized holography represent all forms of generalized holography. The discussion of plane holography given below will present the basic equations underlying the actual Nearfield Acoustic Holography computation algorithms, and will illustrate in detail the departures from conventional holography and the sources of problems in real applications of generalized holography.

For plane holography the separable coordinate system is of course the cartesian system with rectangular coordinates (x,y,z). The surface S (described in section A above) is taken to be the infinite plane defined by $z = z_S$ (a constant) and the infinite hemisphere enclosing the $z > z_S$ half-space. It is assumed that the sources lie in a finite region just below the z_S plane, and that the field which they generate obeys the Sommerfeld radiation condition[2] [i.e., $r(\partial\tilde{\psi}/\partial n - ik\tilde{\psi})$ vanishes on the hemisphere at infinity]. As an aid in understanding, it is useful to assume that the sources are planar, such as vibrating plates, etc., lying in the z_S plane; non-planar sources and depth resolution below the z_S plane will be discussed later.

For expression (7) relating $\tilde{\psi}(x,y,z)$ to $\tilde{\psi}(x,y,z_S)$, we need the Green's function which satisfies the homogeneous Dirichlet boundary condition on z_S;

this is given by[12]

$$G(x,y,z|x',y',z') = \frac{e^{ik\sqrt{(x-x')^2+(y-y')^2+(z-z')^2}}}{\sqrt{(x-x')^2+(y-y')^2+(z-z')^2}} - \frac{e^{ik\sqrt{(x-x')^2+(y-y')^2+(z+z'-2z_S)^2}}}{\sqrt{(x-x')^2+(y-y')^2+(z+z'-2z_S)^2}} \tag{13}$$

The normal derivative $(\partial/\partial z')$ at $z' = z_S$ is

$$-4\pi\, G'(x-x', y=y', z-z_S) \equiv$$

$$\frac{\partial G}{\partial n}(x,y,z|x',y',z_S) = -2\,\frac{\partial}{\partial \alpha}\left[\frac{e^{ik\sqrt{(x-x')^2+(y-y')^2+\alpha^2}}}{\sqrt{(x-x')^2+(y-y')^2+\alpha^2}}\right]_{\alpha=(z-z_S)} \tag{14}$$

so that Equation (7) becomes

$$\tilde{\psi}(x,y,z) = \int\int_{\infty}^{+\infty} \tilde{\psi}(x',y',z_S) G'(x-x', y-y', z-z_S)\, dx'dy' \tag{15}$$

It should be noted that expression (13) is not the free space Green's function[12] which has just one term in the form exp(ikR)/R. Although expression (14) follows this form, the free space Green's function is not used in this boundary value problem. Equation (15) is not an approximate form of Green's theorem with one of the free-space Green's function terms dropped, as is sometimes mistakenly assumed.

Usually the hologram data is not recorded on the sources ($z = z_S$) but rather on a plane $z = z_H > z_S$ above and parallel to the source plane. Evaluating Equation (15) with $z = z_H$ yields

$$\tilde{\psi}(x,y,z_H) = \int\int_{-\infty}^{\infty} \tilde{\psi}(x',y',z_S) G'(x-x', y-y', z_H-z_S)\, dx'dy' \tag{16}$$

where $\tilde{\psi}(x,y,z_H)$ is the hologram data (assumed to be available for all x and y in the z_H plane). Since $z_H - z_S$ is a constant, Equation (16) is a two-dimensional convolution, and $\tilde{\psi}(x',y',z_S)$ can be found in terms of $\tilde{\psi}(x,y,z_H)$ with the convolution theorem. We denote the two-dimensional spatial Fourier transform as $\hat{\psi}$:

$$\hat{\tilde{\psi}}(k_x,k_y,z_H) = \iint_{-\infty}^{\infty} \tilde{\psi}(x,y,z_H) e^{-i(k_x x + k_y y)}\, dx\, dy \tag{17}$$

and the inverse transform as F^{-1}. With the convolution theorem we can rewrite Equation (15) as

$$\tilde{\psi}(x,y,z) = F^{-1}\{\hat{\tilde{\psi}}(k_x,k_y,z_S)\cdot\hat{G}'(k_x,k_y,z-z_S)\} \tag{18}$$

and Equation (16) can be written as:

$$\hat{\tilde{\psi}}(k_x,k_y,z_H) = \hat{\tilde{\psi}}(k_x,k_y,z_S)\cdot\hat{G}'(k_x,k_y,z_H-z_S) \quad . \tag{19}$$

Solving Equation (19) for $\hat{\tilde{\psi}}(k_x,k_y,z_S)$ and substituting in Equation (18) yields:

$$\tilde{\psi}(x,y,z) = F^{-1}\left\{\hat{\tilde{\psi}}(k_x,k_y,z_H)\cdot\left[\frac{\hat{G}'(k_x,k_y,z-z_S)}{\hat{G}'(k_x,k_y,z_H-z_S)}\right]\right\} \tag{20}$$

Equation (20) is the expression which gives the holographic reconstruction of the three-dimensional field $\tilde{\psi}(x,y,z)$ in terms of the (Fourier transformed) hologram data $\tilde{\psi}(x,y,z_H)$.

From Equation (14) the two-dimensional spatial Fourier transform $\hat{G}'$ can be found explicitly:

$$\hat{G}'(k_x,k_y,z) = \begin{cases} e^{iz\sqrt{k^2-k_x^2-k_y^2}} & k_x^2+k_y^2 \le k^2 \quad (21a) \\ e^{-z\sqrt{k_x^2+k_y^2-k^2}} & k_x^2+k_y^2 > k^2 \quad (21b) \end{cases}$$

The interpretation of $\hat{G}'(k_x k_y, z-z_S)$ and its role in Equation (18) is as follows:

The source plane at $z = z_S$ is considered as a superposition of surface waves $\exp(ik_x x + ik_y y)$ with amplitudes $\hat{\tilde{\psi}}(k_x,k_y,z_S)$. Since there are no restrictions on the nature of the sources, then $\hat{\tilde{\psi}}(k_x,k_y,z_S)$ can have non-zero values for any point in the two-dimensional k-space (k_x,k_y). In fact, if the sources are of finite extent in the z_S plane, then $\hat{\tilde{\psi}}(k_x,k_y,z_S)$ must be nonzero for arbitrarily

large values of k_x and k_y.[17] One must then consider both forms of $\hat{G}'(k_x,k_y,z-z_S)$ in Equation (21) and their role in Equation (18). When $k_x^2 + k_y^2 \leq k^2$, then the surface waves in the z_S plane simply couple to ordinary propagating plane waves in the three-dimensional region $z > z_S$. These plane waves have amplitudes (k_x,k_y,z_S), travel in the direction given by the wavector $(k_x,k_y, k^2- k_x^2 - k_y^2)$, and have wavevector maganitude k so as to satisfy the original Helmholz Equation (6). The kernal or "propagator in Equation (18), $\hat{G}'(k_x,k_y,z-z_S) = \exp[i(z-z_S)\sqrt{k^2 - k_x^2 - k_y^2}]$, simply provides the plane-wave phase change in going from the z_S plane to the z plane. The propagating plane wave emerges from the z_S plane at just such an angle so as to exactly match the surface wave in the z_S plane.

When $k_x^2 + k_y^2 > k^2$, then there is no way that one can add a real z-component to (k_x,k_y) and form a three-dimensional plane wave with wavevector magnitude k. If $k_x^2 + k_y^2 > k^2$ then the length of the surface wave is shorter than $\lambda = 2\pi/k$; having a three-dimensional plane wave (of wavelength λ) emerging from the z_S plane at some angle can only match surface waves which have two-dimensional wavelengths greater than or equal to λ. Surface waves with $k_x^2 + k_y^2 > k^2$ must be matched with evanescent waves[18] which have imaginary z-components in their wavevector, and which exponentially decay in the z-direction as $\exp[-(z - z_S)\sqrt{k_x^2 + k_y^2 - k^2}]$. This is correctly represented in Equation (18) with the form of $\hat{G}'$ in Equation (21b). The boundary in k-space which separates the propagating plane wave region from the evanescent wave region is the "radiation circle," defined by $k_x^2 + k_y^2 = k^2$.

The situation described above is illustrated in Fig. 1. In this figure the "FT" dashed lines represent the two-dimensional forward Fourier transform going from an (x,y)-plane in real space to the (k_x,k_y)-plane in k-space, the "IFT" dashed lines represent the inverse Fourier transform, and $k_z \equiv \sqrt{|k^2 - k_x^2 - k_y^2|}$. Features of the source in the z_S plane which vary in space more slowly than λ

get mapped by the FT to points in k-space lying inside the radiation circle; features of the source which vary in space more rapidly than λ get mapped to points in k-space lying outside the radiation circle. The wavefield in a plane a distance z above the z_S plane is determined in k-space by multiplying the amplitudes $\hat{\psi}(k_x,y_y,z_S)$ inside the radiation circle by $\exp(ik_z z)$ (thus surface waves varying more slowly than λ simply undergo a phase change in moving to a plane away from the sources), and by multiplying the amplitudes outside the radiation circle by $\exp(-k_z z)$ (so that surface waves varying more rapidly than λ suffer an exponential decay in amplitude in moving to a plane away from the sources).

Having discussed the role of the propagator $\hat{G}'$ [Equation (21)] in radiation from the z_S plane [Equation (18)], we now consider its action in the expression for holographic reconstruction, Equation (20). By inserting the expression for $\hat{G}'$ [Equation (21)] into Equation (20) we obtain:

$$\tilde{\psi}(x,y,z) = F^{-1}\left[\hat{\psi}(k_x,k_y,z_H)\begin{cases} e^{ik_z(z-z_H)} & , \quad k_x^2+k_y^2 \le k^2 \\ e^{-k_z(z-z_H)} & , \quad k_x^2+k_y^2 > k^2 \end{cases}\right] \tag{22}$$

When $z > z_H$, then Equation (22) is analogous to Equation (18), and it represents the phase change of the propagating plane wave components and the exponential decay of the evanescent wave components in going from the z_H plane outward (away from the sources) to the z plane. When $z < z_H$, then the factor $\exp[-ik_z(z_H-z)]$ reverses the phase change of the propagating plane waves, and the positive exponential $\exp[+k_z(z_H-z)]$ restores the decayed evanescent wave amplitudes to their original values in the z plane.

It should be noted that z_S does not appear in Equation (22), nor will it occur explicitly in any final reconstruction expressions. The role of the surface S in the derivation of generalized holography is only to establish

rigorously the region of validity of the final expressions. In real applications of generalized holography, the z_S surface is the one parallel to the z_H surface which just touches the physical sources or scattering objects.

If we redefine k_z to be a complex function of k_x and k_y as

$$k_z = \begin{cases} \sqrt{k^2 - k_x^2 - k_y^2} & , \quad k_x^2 + k_y^2 \leq k^2 \\ i\sqrt{k_x^2 + k_y^2 - k^2} & , \quad k_x^2 + k_y^2 > k^2 \end{cases} \tag{23}$$

then Equation (22) becomes, with F^{-1} explicitly expressed:

$$\tilde{\psi}(x,y,z) = \frac{1}{(2\pi)^2} \iint_{-\infty}^{\infty} \left[\hat{\tilde{\psi}}(k_x,k_y,z_H) e^{-ik_z z_H} \right] e^{i(k_x x + k_y y + k_z z)} dk_x dk_y \quad . \tag{24}$$

Equation (24) is of the form

$$\tilde{\psi}(x,y,z) = \frac{1}{(2\pi)^2} \iint_{-\infty}^{\infty} \tilde{A}(k_x,k_y) e^{i(k_x x + k_y y + k_z z)} dk_x dk_y \tag{25}$$

which is the general solution of the Helmholz Equation (6) which one would obtain using the method of separation of variables in cartesian coordinates. The two constants of separation are k_x^2 and k_y^2, the mode labels are k_x and k_y, and the product solutions (eigenfunctions) are the propagating plane waves and the evanescent waves:

$$\tilde{u}(k_x,k_y;x,y,z) = \begin{cases} e^{ik_x x} e^{ik_y y} e^{iz\sqrt{k^2 - k_x^2 - k_y^2}} & k_x^2 + k_y^2 \leq k^2 \\ e^{ik_x x} e^{ik_y y} e^{-z\sqrt{k_x^2 + k_y^2 - k^2}} & k_x^2 + k_y^2 > k^2 \end{cases} \tag{26}$$

The reconstruction expressions of generalized holography may be derived quickly from general solutions such as Equation (25). One simply evaluates the general solution at the hologram coordinate, $z = z_H$, and then uses the orthogonality of the product solutions to uniquely solve for the coefficients $\tilde{A}(k_x k_y)$ in terms of the hologram data $\tilde{\psi}(x,y,z_H)$. The result is an expression of the form of Equation (24). This separation of variable and eigenfunction technique

will be used to derive the expressions of generalized holography for coordinate systems other than cartesian; in non-cartesian coordinate systems the Green's function is known only in terms of an eigenfunction expansion so that no convolution expressions analogous to Equation (15) are available, and only expressions analogous to Equation (25) can be used. For the derivation of the expressions of plane generalized holography [Equation (18) - (22)], it would have been easier to use separation of variables in cartesian coordinates and expansions in terms of the eigenfunctions of Equation (26); however, the use of the real-space Green's function $G'(x-x',y-y',z-z_S)$ [Equation (14)] in the convolution expression (15) will be necessary in dealing with the problem of a finite hologram aperture in real applications of plane generalized holography.

At this point the wavelength resolution limit of conventional holography should be discussed. The "resolution" of a field refers to how rapidly the field varies in space. It may be quantitatively measured by Fourier transforming the field in some direction (for example the x-direction) and then examining the amplitudes for the different "spatial frequencies" k_x. If in any direction there are no amplitudes larger than some pre-defined cutoff value for spatial frequencies beyond some value k_{max}, then the minimum distance over which the field varies in space, or the resolution distance, is $R \equiv 2\pi/k_{max}$. In generalized holography the resolution is determined by the values of k_x and k_y for which $\tilde{\psi}(k_x,k_y,z_S)$ has a significant magnitude. As already discussed, if there are no limits on the nature of the sources, then $\hat{\tilde{\psi}}(k_x,k_y,z_S)$ may have finite amplitudes for arbitrarily large values of k_x and k_y. In the reconstruction expressions of generalized holography (e.g., Equation 24) the intergrals in k-space extend over the infinite domain, so that generalized holography has no intrinsic resolution limit; as already stated the reconstruction expressions of generalized holography are exact. The actual resolution limits of practical generalized holography

will be discussed in the section on actual implementation; however the resolution limit of conventional holography may be obtained immediately. In typical conventional holography, holograms are recorded at a distance d in the Fraunhofer or Fresnel zone of the sources (many wavelengths away from the sources, $d >> \lambda$) so that the hologram represents the Fourier transform of the sources $\hat{\hat{\psi}}(kx/d, ky/d, z_s)$[2]. That is, the forward Fourier transform of generalized holography is performed by the field propagation itself. However, what is wrong here (and ignored in most textbooks on holography) is that this procedure does not work for the evanescent wave components. The reasons that the evanescent waves are ignored is because they decay (by the factor $\exp[-k_z(z-z_s)]$) to an unmeasurable level in the Fraunhofer or Fresnel zone. Taking $2\pi/\lambda$ as a typical value for k_z, and taking 2λ for $(z-z_s)$, we have $\exp[-(2\pi/\lambda)(2\lambda)] = \exp(-4\pi) \approx 10^{-6}$, so that the evanescent waves may decay by six orders of magnitude within only two wavelengths from the source. On the other hand the propagating wave components maintain their amplitudes and only change phase in traveling to the farfield (thus phase is more important in conventional holography). In conventional holography (optical and acoustical) only the propagating wave components ($\hat{\hat{\psi}}(k_x, k_y, z_s)$ with $k_x^2 + k_y^2 \leq k^2$) are measured, and only these are used in the reconstruction.[2-5] With only these components the maximum spatial frequency is $k_{max} = k = 2\pi/\lambda$, and the resolution distance is $R = \lambda/k_{max} = \lambda/2$; thus the resolution of conventional holography is limited by the wavelength of the radiation. If better resolution is to be obtained in generalized holography, then the evanescent wave components must be measured; furthermore, the reconstruction expressions (including the Fourier transforms) must be evaluated numerically, since there are no techniques in Fourier optics which can reconstruct the evanescent wave components.

E. Calculation of other quantities

1. Field gradient (particle velocity field)

Once the three-dimensional wave field $\tilde{\psi}(x,y,z)$ has been determined, other quantities such as the field gradient $\vec{\nabla}\tilde{\psi}$ can be determined. In acoustics, where $\tilde{\psi}$ is the sound pressure field, the particle velocity field can be calculated from

$$\vec{\tilde{V}}(\vec{r}) = \vec{\nabla}\tilde{\psi}(\vec{r})/i\mu ck \tag{27}$$

where μ is the fluid mass density. By taking the gradient operator inside the integral in Equation (24), the expressions for the three particle velocity components V_η, $\eta = x,y,z$, become

$$\tilde{V}_\eta(x,y,z) = \frac{1}{4\pi^2\mu c}\int\int_{-\infty}^{\infty}\hat{\tilde{\psi}}(k_x,k_y,z_H)\left[\frac{k_\eta}{k}e^{ik_z(z-z_H)}\right]e^{i(k_x x+k_y y)}dk_x dk_y \tag{28}$$

It is important to remember that in expressions such as (24) and (28), k_z is a complex function of k_x and k_y.

At this point it is worth considering solving Equation (20) for $\tilde{\psi}(k_x,k_y z_H)$ in terms of $\tilde{V}_z(x,y,z_S)$ and using this in Equation (24). The result is

$$\tilde{\psi}(x,y,z) = \frac{\mu c}{4\pi^2}\int\int_{-\infty}^{\infty}\hat{\tilde{V}}_z(k_x,k_y,z_S)\left[\frac{1}{\sqrt{k^2-k_x^2-k_y^2}}e^{ik_z(z-z_S)}\right]e^{i(k_x x+k_y y)}dk_x dk_y \tag{29}$$

which is the same result which would be obtained if the original problem had been specified with Neuman instead of Dirichlet boundary conditions. [This is the expression which would be used to predict the radiation from a planar vibrator; the surface velocity $v_z(x,y,z_S)$ might be determined from a structural analysis program.] The important thing to notice here is the appearance of k_z (written out as $\sqrt{k^2-k_x^2-k_y^2}$ in Equation 29) in the denominator of the kernal

(the term in brackets); on the radiation circle ($k_x^2 + k_y^2 = k^2$) the kernal is singular. This singular behavior must be kept in mind when one attempts to evaluate Equation (29) using conventional computer techniques; this will be discussed further in the section on actual implementation.

As already mentioned, finite aperture effects may be more readily handled if one uses real-space convolution expressions rather than the Fourier transform expressions such as Equation (29). If the convolution theorem is applied to Equation (29) and the kernel is transformed analytically, then one obtains

$$\tilde{\psi}(x,y,z) = \frac{1}{4\pi} \iint_{-\infty}^{\infty} i\mu ck\ \tilde{v}_z(x',y',z_S) \left[2\ \frac{e^{ik\sqrt{(x-x')^2+(y-y')^2+(z-z_S)^2}}}{\sqrt{(x-x')^2+(y-y')^2+(z-z_S)^2}} \right] dx'dy' \quad (30)$$

Equation (30) is the real-space convolution expression for the solution to the Neuman boundary value problem, i.e., Equation (12) in cartesian coordinates; the term in brackets is the Green's function evaluated at z_S, and $i\mu ck\ v_z(x',y',z_S) = \partial\tilde{\psi}/\partial z$ on z_S.

2. Farfield directivity pattern

A farfield directivity pattern can be determined if the cartesian coordinates are written in terms of spherical coordinates r, θ, ϕ defined by

$$x = r \sin\theta \cos\phi \quad (31a)$$

$$y = r \sin\theta \cos\phi \quad (31b)$$

$$z = z_S = r \cos\theta \quad (31c)$$

A complex directivity function $\tilde{D}(\theta,\phi)$ may be defined by

$$\tilde{\psi}(r \sin\theta \cos\phi,\ r \sin\theta \sin\phi,\ r \cos\theta) \underset{r\to\infty}{\longrightarrow} \tilde{D}(\theta,\phi)\ \frac{\exp(ikr)}{r} \quad (32)$$

If expression (30) is used for $\tilde{\psi}$ with the large r approximation

$$\sqrt{(x-x')^2 + (y-y')^2 + (z-z_S)^2} \approx r - x' \sin\theta \cos\phi - y' \sin\theta \sin\phi \qquad (33)$$

then one obtains

$$\tilde{D}(\theta,\phi) = i\mu ck\, \hat{\tilde{v}}_z(k \sin\theta \cos\phi,\ k \sin\theta \sin\phi,\ z_S) \quad . \qquad (34)$$

Using $\tilde{V}_z$ from the Fourier transform of Equation (28) (with $z = z_S$) yields

$$\tilde{D}(\theta,\phi) = k \cos\theta\, \hat{\tilde{\psi}}(k \sin\theta \cos\phi,\ k \sin\theta \sin\phi,\ z_H) i e^{-ik \cos\theta (z_H - z_S)} \quad . \qquad (35)$$

Thus the farfield directivity pattern can be found from the Fourier transform of the hologram data. Usually the phase factor is ignored. It is important to note that since $(k \sin\theta \cos\phi)^2 + (k \sin\theta \sin\phi)^2 = (k \cos\theta)^2 \leq k^2$, then the farfield directivity pattern depends only on those components $\tilde{\psi}(k_x, k_y, z_H)$ which lie inside the radiation circle.

3. Second order quantities (acoustic vector intensity field, total power radiated)

From the three-dimensional field ψ and its gradient $\vec{\nabla}\psi$ second-order products may be determined. A particularly important example is the acoustic vector intensity field, defined by

$$\vec{S}(\vec{r}) = \frac{1}{T} \int_{t_0}^{t_0+T} \psi(\vec{r},t) \vec{V}(\vec{r},t)\, dt \qquad (36)$$

where ψ and $\vec{V}$ are the sound pressure and particle velocity fields, and T is a suitable time scale[13] for noise sources or the period for harmonic sources. With the assumptions required to make Equation (5) an equality (i.e., harmonic sources), then Equation (34) becomes a sum of independent frequency terms, each contributing to the intensity field an amount:

$$\vec{S}(\vec{r}) = \frac{1}{2} \mathrm{Re}\ [\tilde{\psi}(\vec{r}) \vec{V}^*(\vec{r})] \qquad (37)$$

This can be calculated from the hologram data using Equations (22) and (28).

By integrating the normal component of the intensity field over a suitable surface, the total power radiated may be obtained. For plane holography, the total power radiated into the half-space away from the source plane is

$$P \equiv \frac{1}{2} \mathrm{Re} \iint_{-\infty}^{\infty} \tilde{\psi}(x,y,z)\tilde{V}_z^*(x,y,z)\,dxdy \tag{38}$$

for any $z \geq z_S$. For some sources it may be known that $\tilde{\psi}$ or $\tilde{V}_z$ vanishes except over some finite region, so that Equation (36) may be evaluated numerically. In any case, Equation (36) may be rewritten using the identity

$$\iint_{-\infty}^{\infty} \tilde{\psi}(x,y,z)\tilde{V}_z^*(x,y,z)\,dxdy = \frac{1}{4\pi^2} \iint_{-\infty}^{\infty} \hat{\tilde{\psi}}(k_x,k_y,z)\hat{\tilde{V}}_z^*(k_x,k_y,z)\,dk_x dk_y \tag{39}$$

so that

$$P = \frac{1}{8\pi^2} \mathrm{Re} \iint_{-\infty}^{\infty} \hat{\tilde{\psi}}\ (k_x,k_y,z)\ \hat{\tilde{V}}_z^*(k_x,k_y,z)\,dk_x dk_y \tag{40}$$

From Equation (24) we have

$$\hat{\tilde{\psi}}(k_x,k_y,z) = \hat{\tilde{\psi}}(k_x,k_y,z_H)e^{ik_z(z-z_H)} \tag{41}$$

and from Equation (28) we have

$$\hat{\tilde{V}}_z(k_x,k_y,z) = \frac{1}{\mu C} \hat{\tilde{\psi}}(k_x,k_y,z_H)\ \frac{k_z}{k}\ e^{ik_z(z-z_H)} \tag{42}$$

Keeping in mind that $k_z = \sqrt{k^2-k_x^2-k_y^2}$ is a complex function, we have

$$\mathrm{Re}\left[\hat{\tilde{\psi}}(k_x,k_y,z)\hat{\tilde{V}}_z^*(k_x,k_y,z)\right] = \begin{cases} \frac{1}{\mu C}\ |\hat{\tilde{\psi}}(k_x,k_y,z_H)|^2\ \sqrt{1-(k_x^2+k_y^2)/k^2} & k_x^2+k_y^2 \leq k^2 \\ 0 & k_x^2+k_y^2 > k^2 \end{cases} \tag{43}$$

Now

$$P = \frac{1}{8\pi^2\mu C} \iint_{k_x^2+k_y^2 \leq k^2} |\hat{\tilde{\psi}}(k_x,k_y,z_H)|^2\ \sqrt{1-(k_x^2+k_y^2)/k^2}\ \ dk_x dk_y \tag{44}$$

Like the farfield directivity pattern, the total power radiated depends only on the components $\hat{\tilde{\psi}}(k_x,k_y z_H)$ which lie inside the radiation circle. When

Equations (33) and (42) are evaluated numerically using actual hologram data, care must be taken to insure that there is a sufficient density of data points inside the radiation circle. This will be discussed further in the section on actual implementation.

F. Cylindrical holography

As demonstrated by Equations (24) and (25), the expressions of generalized holography may be found by using separation of variables to find the general solution to the Helmholz Equation (6) and then using the hologram data and the orthogonality of the eigenfunctions to find the unique solution. In cylindrical coordinates (ρ,ϕ,z) the general solution (for sources contained just inside the surface S given by $\rho = \rho_S$ and radiating outward) is

$$\tilde{\psi}(\rho,\phi,z) = \sum_{m=-\infty}^{\infty} \int_{-\infty}^{\infty} \tilde{A}_m(k_z) e^{im\phi} e^{ik_z} H_m(k_\rho \rho)\, dk_z \tag{45}$$

where m is an integer, $\tilde{A}_m(k_z)$ are the eigenfunction amplitudes to be determined from the hologram data, $k_\rho = \sqrt{k^2-k_z^2}$ is a complex quantity analogous to k_z in Equation (23), and $H_m(k_\rho \rho)$ is the Hankel function (when $k_z \leq k$) or modified Hankel function (when $k_z > k$) behaving asymptotically as $\exp(i\sqrt{k^2-k_z^2}\,\rho)$ or $\exp(-\sqrt{k_z^2-k^2}\,\rho)$. The modified Hankel function solutions are analogous to the evanescent wave components of the cartesian coordinate eigenfunctions.

The eigenfunction amplitudes $\tilde{A}_m(k_z)$ in Equation (43) can be found from hologram data measured on the surface $\rho = \rho_H$, where $\rho_H \geq \rho_S$. The orthogonality of the eigenfunctions is such that

$$\int_{-\infty}^{\infty} dz \int_0^{2\pi} d\phi \left[e^{im\phi} e^{ik_z z}\right]\left[e^{im'\phi} e^{ik'_z z}\right]^* = 4\pi^2 \delta_{mm'} \delta(k_z - k'_z) \tag{46}$$

Evaluating Equation (43) at $\rho = \rho_H$ and using Equation (44) to solve for $\tilde{A}_m(k_z)$ yields

$$\tilde{A}_m(k_z) = \frac{1}{2\pi} \hat{\tilde{\psi}}_m(k_z,\rho_H)/H_M(k_\rho\rho_H) \tag{47}$$

where

$$\hat{\tilde{\psi}}_m(k_z,\rho_n) = \frac{1}{2\pi} \int_{-\infty}^{\infty} dz \int_0^{2\pi} d\phi\ \tilde{\psi}(\rho_u,\phi,z) e^{-im\phi} e^{-ik_z z} \tag{48}$$

Substituting $\tilde{A}_m(k_z)$ in Equation (43) yields

$$\tilde{\psi}(\rho,\phi,z) = \frac{1}{2\pi} \sum_{m=-\infty}^{\infty} \int_{-\infty}^{\infty} \hat{\tilde{\psi}}_m(k_z,\rho_u) e^{im\phi} e^{ik_z z} \left[\frac{H_m(k_\rho\rho)}{H_m(k_\rho\rho_u)}\right] dk_z \tag{49}$$

which is the analog of Equation (24). Again it should be kept in mind that $k_\rho = \sqrt{k^2-k_z^2}$ is a complex function of k_z. Other quantities such as the field gradient, etc. may be calculated from $\tilde{\psi}(\rho,\phi,z)$ as for the cartesian coordinate solution. The solution (47) is valid for $\rho \geq \rho_S$, where $\rho = \rho_S$ is the smallest cylindrical surface which just touches the physical sources or scattering surfaces.

G. Spherical holography

In spherical coordinates (r,θ,ϕ), the general solution (for sources contained within a spherical surface S defined by $r = r_S$ and radiating outward) is

$$\tilde{\psi}(r,\theta,\phi) = \sum_{\ell=0}^{\infty} \sum_{m=-\ell}^{\ell} \tilde{A}_{\ell m}\, Y_{\ell m}(\theta,\phi) h_\ell(kr) \tag{50}$$

where ℓ and m are integers, the $Y_{\ell m}(\theta,\phi)$ are the spherical harmonics, and $h_\ell(kr)$ is the spherical Bessel function behaving asymptotically as exp(ikr). It is interesting to note that there are no exponentially decaying functions in this solution. The eigenfunction amplitudes $\tilde{A}_{\ell m}$ can be determined from hologram data on a spherical surface $r = r_H$, with $r_H > r_S$, by using the orthonormalization of the spherical harmonics. One obtains

$$\tilde{A}_{\ell m} = \hat{\psi}_{\ell m}(r_H)/h_\ell(kr_H) \tag{51}$$

where

$$\hat{\psi}_{\ell m}(r_H) \equiv \int_0^{\pi} \sin\theta \, d\theta \int_0^{2\pi} d\phi \; \tilde{\psi}(r_H,\theta,\phi) Y^*_{\ell m}(\theta,\phi) \quad . \tag{52}$$

Substituting $\tilde{A}_{\ell m}$ into Equation (48) yields

$$\tilde{\psi}(r,\theta,\phi) = \sum_{\ell=0}^{\infty} \sum_{m=-\ell}^{\ell} \hat{\psi}_{\ell m}(r_N) Y_{\ell m}(\theta,\phi) \left[\frac{h_\ell(kr)}{h_\ell(kr_H)}\right] \tag{53}$$

which is the analog of Equations (24) and (47).

V. ACTUAL IMPLEMENTATION

A. General

The implementation of generalized holography in an actual system involves acquisition of the hologram data and evaluation of the various expressions of generalized holography. Because the features of the (hardware) system used for actual data acquisition depend on many extraneous design variables, few general comments may be made about data acquisition. On the other hand a number of interesting general general comments can be made concerning the numerical evaluation of the holography expressions. The following paragraphs discuss the general features, problems, limitations, etc., associated with the actual implementation of generalized holography. In these paragraphs it should be assumed that the comments are about plane holography in particular but may be generalized to other coordinate systems unless otherwise stated. The aspects of a particular hardware system (used for data acquisition and processing) will be described in the section on Nearfield Acoustic Holography.

B. Data acquisition

Concerning data acquisition, it can be assumed that the major temporal frequency components are sampled at the Nyquist rate or faster, and that any other components at higher frequencies are filtered to a sufficiently small "noise" level. The time-sampled data may then be analyzed to produce the temporal frequency complex amplitudes $\psi(\vec{r}_H)$, as discussed in Section IV.A. In theory, the hologram data must be known as a continuous function (i.e., known at all points $\vec{r}_H$) over the hologram surface H which may be infinite in extent (spherical holography being one exception). In practice, the hologram data can only be sampled at discrete points on a surface of finite extent (referred to as the hologram aperture). As far as the discrete sampling is concerned, one must be

certain that the field $\tilde{\psi}(\vec{r}_H)$ is being sampled at the spatial Nyquist rate. It should be recalled that any spatial frequencies of the source which exceed those of the characteristic radiated wavelengths exponentially decay with distance from the source. Thus spatial sampling is provided with a natural filter; as an empirical rule-of-thumb, we find that if the hologram sampling is done at a distance d from the source, then the distance between sampling points should be no larger than d [see section Example of Implementation: Nearfield Acoustic Holography]. Discrete spatial sampling does not result in any unusual problems in generalized holography. On the other hand, the finite hologram aperture does result in fundamental problems which require special processing techniques. Of course, the holography expressions which involve integrals over infinite domains in space (as in plane and cylindrical holography) necessitate that some assumption be made about the hologram (or source) data which lies outside the finite hologram aperture. Practical limitations notwithstanding, it can be assumed that the hologram aperture may be made sufficiently larger than the sources (of finite extent) so that the field on the surface beyond the aperture is not significantly different from zero. This is a reasonable assumption for laboratory studies, but other techniques may be required for field measurements, as discussed in the section on Further Developments. The special processing required even when the field is zero outside the aperture is discussed in subsection D below.

In addition to being finite and discrete, the actual measured hologram data will contain some intrinsic error including background sound, electronic noise, calibration errors, etc. The error level may be characterized by a dynamic range D definied by

$$D = 20 \log_{10}(M/E) \tag{54}$$

where M is the maximum field amplitude which is measured and E is the amplitude of the error. It is interesting that this dynamic range plays a role in determining the spatial resolution of generalized holography, as discussed in the next subsection.

C. Resolution

A discussion of the resolution of the reconstructed fields of generalized (plane) and conventional holography was presented in section IV.D. The minimum resolvable distance is on the order of $R \equiv \pi/k_{max}$, where k_{max} is the highest spatial frequency for a measurable Fourier component $\tilde{\psi}(k_x k_y, z_H)$. In conventional optical and acoustical holography no evanescent waves are used in the field reconstructions so that $k_{max} = k$ and $R = \lambda/2$. In actual implementations of generalized holography, the hologram is uniformly sampled at discrete points in space; from the Nyquist theorem $k_{max} \leq \pi/a$, were a is the distance between the spatial sampling points, so that $R \geq a$. The sampling lattice contstant a is only a lower limit for R because k_{max} may be further limited by the ability of the hologram recording medium to measure all of the necessary evanescent wave components, as discussed below.

In order for generalized holography to surpass conventional holography in resolution, it is necessary to measure some evanescent wave components so that k_{max} will exceed k. The evanescent wave components decay rapidly with distance from the source, and some of the components, in traversing the distance from the source to the hologram, will decay to a level below the error level E of the hologram recording system. These evanescent wave components cannot be used in the reconstruction, and this sets a limit on k_{max}. In order to quantify this, we assume that the source, at z_S, has propagating and evanescent

wave components with equal amplitudes; that is $A \equiv$ (typical $|\hat{\tilde{\psi}}(k_x, k_y, z_S)|$) is the same for some $k_x^2 + k_y^2 \leq k^2$ as for some $k_x^2 + k_y^2 > k^2$. Since the propagating wave components maintain their amplitude in traveling to the hologram plane, then $A \leq M$, where M is defined in subsection B above. On the other hand, the evanescent wave components in the hologram plane $z_H > z_S$ will have amplitudes $A \exp[-\sqrt{k_x^2 + k_y^2 - k^2}\,(z_H - z_S)]$. In order for these to be used in the reconstruction the amplitude must be above the error level E:

$$A \exp\left[-\sqrt{k_x^2 + k_y^2 - k^2}\,(z_H - z_S)\right] > E \quad . \tag{55}$$

Using Equation (54) defining the dynamic range D of the hologram recording system and the relation $A \leq M$, we obtain

$$(k_x^2 + k_y^2) < k^2 + \left[\frac{D \ln 10}{20(z_H - z_S)}\right]^2 \tag{56}$$

The expression on the right hand side of the inequality (56) is the upper limit of usable values of $(k_x^2 + k_y^2)$ and hence is k_{max}^2. The minimum resolvable distance $R = \pi / k_{max}$ is now

$$R = \left\{ \frac{4}{\lambda^2} + \left[\frac{D \ln 10}{20\pi(z_H - z_S)}\right]^2 \right\}^{-1/2} \tag{57}$$

Since the dynamic range term is usually much larger than $4/\lambda^2$, we have

$$R \simeq \frac{20\pi(z_H - z_S)}{D \ln 10}$$

Thus in actual implementation of generalized holography, good resolution is obtained by having a precise recording system (large dynamic range D) and by

measuring as close to the sources as possible (small $z_H - z_S$). Measuring close to the sources is no problem in generalized holography since no use is made of Fourier optics and there is no requirement for recording in the Fraunhofer or Fresnel zone.

D. Finite aperture effects: Wrap-around error

As already mentioned, practical data acquisition results in the hologram being finite in size and discretely sampled. The processing of the hologram field must also be finite and discrete in nature; that is, even if the hologram data could be assigned some assumed a' priori values outside the data acquisition range, the time and space limitations of the data processing hardware would still restrict the hologram field to be finite in size. This finite aperture restriction leads to interesting effects, in particular an error referred to as wrap-around,[19] which fortunately can be controlled with proper processing techniques. The wrap-around error and the techniques used to avoid it are discussed in this section.

To emphasize that the wrap-around error results from improper data processing rather than insufficient data acquisition, we shall assume that the actual field in the hologram plane is negligible for points (x,y) outside the square region defined by $x = \pm L/2$ and $y = \pm L/2$. Thus $\tilde{\psi}(x,y,z_H)$ for (x,y) within the finite L x L aperture accurately represents the full hologram plane.

The expressions of plane and cylindrical holography involve Fourier transforms which are of course numerically evaluated with finite Fourier transforms and with the FFT computer alogrithm in particular. The field $\tilde{\psi}(x,y,z_H)$ inside the L x L hologram aperture is represented by the discrete series:

$$\tilde{\psi}_L(x,y,z_H) \equiv \sum_{m=0}^{\infty} \sum_{n=0}^{\infty} \hat{\psi}_{m,n}(z_H) e^{i \frac{2\pi}{L}(mx+ny)} \tag{59}$$

where $\hat{\tilde{\psi}}_{m,n}(z_H)$ is proportional to $\hat{\tilde{\psi}}(k_x,k_y z_H)$ with $k_x = (m-N/2)\pi/L$, and $k_y = (n-N/2)\pi/L$, and N is an integer limited by reasonable computation times. This series evaluates to $\tilde{\psi}(x,y,z_H)$ exactly at a set of points inside the L x L aperture, but outside the aperture it represents not the actual (negligibly small) hologram field but rather the periodic extension of the field inside the aperture. This periodic extension is illustrated in Fig. 2a; the small center square represents the L x L aperture and the localized hologram field within it, and the set of nine duplicate squares represents a portion of the infinite periodic extension. This extended field looks like a field generated by the actual source and an infinite number of image sources.

Equation (16) shows that propagation of the field away from a plane involves the convolution of the Green's function with the field in that plane. The Green's function, of approximate form exp(ikR)/R (illustrated in Fig. 2b) has infinite extent (indicated by the arrows in Fig. 2b). If this is convolved with the periodic extension of the field (Fig. 2a), then contributions from the images outside the L x L aperture will leak, or "wrap-around," into the reconstructed field inside the aperture. That is, the Green's function propagates the field from not only the original source, but from all the image sources as well. If one is reconstructing the field in a plane close to the hologram plane [$|z - z_H| \ll L$] then there is negligible error. However, when $(z - z_H) \sim L$, then considerable wrap-around error may result.

How the wrap-around error may be eliminated is illustated in Fig. 2c and 2d. The first step, shown in Fig. 2c, is to surround the L x L aperture with a "guard-band" of zeroes, forming a 2L x 2L aperture. The discrete series representing this field is

$$\tilde{\psi}_{2L}(x,y,z_H) \equiv \sum_{m=0}^{2N} \sum_{n=0}^{2N} \hat{\tilde{\psi}}_{m,n}(z_H) e^{i\frac{\pi}{L}(mx+ny)} \tag{60}$$

which has images as $\tilde{\psi}_L$ has, but they are farther apart. However, pushing the images farther away does little to solve the wrap-around problem because there are an infinite number of images, and they may constructively interfere inside the reconstruction aperture. What solves the problem is the use of truncated Green's function defined by

$$G_T(x,y,z) = \begin{cases} G'(x,y,z) & \text{if } -L \le x \le L \text{ and } -L \le y \le L \\ 0 & \text{otherwise} \end{cases} \tag{61}$$

which is illustrated in Fig. 2d. For points (x,y) inside the original L x L aperture one has

$$\iint_{-\infty}^{\infty} \tilde{\psi}(x',y',z_H) G'(x-x',y-y',z-z_H)\,dx'dy' = \iint_{-L}^{L} \tilde{\psi}_{2L}(x',y',z_H) G_T(x-x',y-y',z-z_H)\,dx'dy' \tag{62}$$

With $-L/2 \le x \le L/2$ and $-L/2 \le y \le L/2$, then the truncated Green's function G_T ignores the images of $\tilde{\psi}_{2L}$. Thus calculating the finite convolution on the right-hand side of Equation (62), which involves the discrete series $\tilde{\psi}_{2L}$, yields exact reconstructions, with no wrap-around error, so long as one only reconstructs inside the "duct" enclosing the original L x L hologram.

In performing actual calculations, the convolution on the right-hand-side of Equation (62) is put into discrete form and evaluated using forward and inverse FFT's. Making the convolution integral discrete involves some approximations and these introduce small errors in the reconstructions. The actual numerical processing of the other quantities which can be determined with generalized holography also involve approximations and small errors. There are a number of different ways of making these approximations and it is found that some procedures result in smaller errors. The development of the techniques to minimize the wrap-around and other errors, and the optimization of their computer algorithms has been accomplished by graduate student W. A. Veronesi[20] and will be published in a second paper.

E. Zoom imaging

As discussed in the previous section, the wrap-around error can be avoided if the reconstruction volume is confined within a duct enclosing the L x L aperture. For reconstructions in the nearfield of the sources the size of this area is usually more than adequate. However for reconstructions out to the farfield a much larger aperture would be desirable. Furthermore, having a larger aperture means that there is a higher density of discrete points in k-space [the distance between points in k-space is π/L], and this may be necessary for calculating quantities such as the farfield directivity and the total power radiated. It should be recalled that these quantities involved $\hat{\tilde{\psi}}(k_x k_y, z_H)$ at points only inside the radiation circle. For low frequency sources, the hologram aperture may be only a few wavelengths in size, and this means that there may be only a few discrete (k_x, k_y) points inside the radiation circle, as illustrated in Fig. 3a; such a low density of points inside the radiation circle may be inadequate for calculating the directivity pattern and the total power radiated.

In order to increase the aperture size one could increase the size of the guard band of zeroes, making the effective aperture size KL x KL. Equivalently, one could convolve $\hat{\tilde{\psi}}(k_x, k_y, z_H)$ in k-space with a $\sin\alpha/\alpha$ type function[14] in order to intersperse discrete points in k-space. Unfortuntely the first technique would require a two-dimensional FFT on a very large data set, and the second would require multiplication by an even larger matrix; both would necessitate prohibitively long computation times.

However, it should be noted that the calculations which require a larger aperture (or higher density of points in k-space) only require a higher density of k-space points inside the radiation circle (since reconstructions beyond a few wavelengths contain virtually no evanescent waves). It is possible to reformulate the k-space convolution technique so that it only intersperses data points within

the radiation circle, as shown in Fig. 3b. In a reasonable amount of computation time all of the original N^2 k-space points (as in Fig. 3a) may be relocated inside the radiation circle (as in Fig. 3b.) With this high density of k-space points, a much larger aperture may be obtained beyond the nearfield. The procedure for enlarging the aperture size is referred to as zoom imaging;[21] a paper describing the computer algorithm for this process is in preparation.

VI. EXAMPLE OF IMPLEMENTATION: NEARFIELD ACOUSTIC HOLOGRAPHY

A. Introduction

In this section we shall describe a sound radiation measurement system, called Nearfield Acoustic Holography (NAH), which utilizes the principles of generalized holography. At The Pennsylvania State University two NAH systems, one for airborne sound and the other for underwater sound, are being used for a wide range of research studies. Several NAH systems are being, or have been, constructed at other laboratories by graduate degree candidates trained at Penn State: Earl Williams has developed a system at the Naval Research Laboratories in Washington, D.C., Bill Strong is constructing a facility at Steinway Piano, and Toshi Mitzutani is developing a system at the Technics Company in Japan. Each system has its own data acquisition features and innovations, but all share the common feature of digital reconstructions based on the principles of generalized holography. Another system employing generalized holography in spherical coordinates has been independently developed by G. A. Weinreich[22] at the University of Michigan, Ann Arbor. The use of FFT methods for modeling sound radiation im cartesian and cylindrical geometries has been studied by Stepanishen and Chen.[23]

B. The NAH system for airborne sound

The Penn State NAH system for airborne sound uses a large two-dimensional open array of microphones. An early system, constructed with the assistance of research associate E. G. Willilams and graduate students W. Y. Strong, T. B. Beyer and D. J. Bowen, had data acquisition electronics which were adequate for only single frequency sound radiation measurements and had data processing algorithms which were relatively slow and inefficient. Recently the data acquisition and processing system has been completely rebuilt[24] so that real-time measurements on wide-band noise sources are now possible; with this system one may study the effects of noise source temporal and spatial coherence

on the acoustic vector intensity field (energy flow patterns) for application in panel design, radiation cancellation, etc.

Figure 4 shows a representation of the NAH airborne sound system. The microphone array is constructed with a square aluminium I-beam frame, approximately 3 m on a side. Attached to the frame is a 16 x 16 lattice-work of 0.8 mm steel wires. The microphones (256 identical units) are located at the intersections of the wires. With a microphone size of ~1 cm (much smaller than the typical 1 m wavelengths studied) and a spacing of 0.18 m, a suitably open (transparent) array is formed. The sound source to be studied is located just a few centimeters below the microphones, so that the array is in the extreme nearfield of the source and can measure the evanescent wave components. The sources are typically ~1 m in size, so that the 3 m array at a distance of ~2 cm subtends a large solid angle ($\lesssim 2\pi$ steradians) from the sources. Thus the source directivity and total power radiated into the half-space above the source can be adequately measured.

The signals from the microphones are routed through a multiplexer to a 4 MHz analog-to-digital converter, and the digitized data are stored in a high-speed buffer memory. The digitized data set consists of 256 time sequences recorded simultaneously at the 256 microphone sites. Once the hologram is recorded (in a fracation of a second) the contents of the buffer memory is transferred through an on-line minicomputer to an attached array processor. A temporal FFT is performed on each of the time sequences producing a two-dimensional (over the hologram (x,y) spatial coordinates) complex data set for each of the temporal frequencies. Each of the 2-D spatial data sets is processed as described in the theory sections. The array processor greatly reduces the time required not only for the temporal and 2-D complex FFT's, but also for the calculation of the Green's functions, window functions, and three-dimensional graphics hidden-line plots. The graphics output is transmitted to

a vector-graphics system which has a much higher resolution and drawing rate than conventional raster-scan systems; with the vector graphics system hidden-line plots may be redrawn in 1/60 second, thus permitting motion-picture views of the holographic reconstructions. This is particularly useful for viewing the motion of a virating structure (in slow motion and with exaggerated displacements) and correlating this motion with features of the holographically reconstructed radiated sound field.[24]

For most sound sources, the density of data points can be greatly increased by spatially interspersing measurements. That is, after recording one set of data, the entire microphone array is translated one-eighth of the distance between the microphones and data are again recorded; the array is then translated another one-eighth distance, data is recorded, and this is repeated in an 8 x 8 pattern in the square areas between the microphones. The result is a 128 x 128 data set with a distance of only ~2 cm between sample points in space. The microphone array translation is carried out completely under the control of the on-line minicomputer using the system of servo motors illustrated in Fig. 4; this system was developed by graduate student Toshi Mizutani.

As indicated in Fig. 4, the timing of the signal multiplexing and digitizing is controlled by separate electronics rather than by the on-line minicomputer. This arrangement permits data acquisition and data processing to be performed in parallel.

In order to record a hologram for a wide-band noise source, the signals from the microphones must be digitized simultanesously, at least on the acoustic time scale of ~0.3 ms. Having 256 individual cables connecting the array microphones to 256 analog-to-digital (A/D) converters would be cumbersome and impractical; a multiplexing system is used instead. Each microphone unit in the array has its own 60 dB amplifier, remotely selectable 20 dB attenuator (to prevent clipping of loud sources), low pass filter, and an output multiplexing switch. In the array, the switches from a column of 16 microphones

are connected in parallel to a "signal" cable, and the gates of 16 switches in a row (orthogonal to the columns) are connected in parallel to a "gate" cable. When one of the gate cables is activated, the signals of the 16 microphones in that row appear on the 16 signal cables. A second stage of multiplexing (located at the corner of the array frame in Fig 3) directs each signal cable in turn to the A/D converter. Repeating this process for each of the 16 gate cables samples the entire array. One such sampling of the array produces one sampling point in each of the 256 time sequences; the array sampling is repeated every 0.3 ms to produce the complete time sequence. The low pass filters in the microphone units prevent time domain aliasing beyond the Nyquist frequency.

In order to sample the entire array in ~0.3 ms the microphone signals must be switched and allowed to settle within ~1 μs. In designing the multiplexing electronics great care must be taken to prevent switching transients from inducing large errors in the microphone signals. The gates of the multiplexing switches are controlled by digital circuits which induce large transients in the ground lines; this digital ground must therefore be isolated from the analog ground of the microphone array. Also, steps must be taken to prevent ringing in the long cables used in the array. After considerable effort Penn State graduate student Donald Bowen[25] was able to develop a data acquisition system which settled to within the digitizing precision (~0.1%) within the 1 μs time limit.

Another important factor in the microphone array operation is calibration. When performing reconstructions back toward the sources, the positive exponential factors of the inverse Green's function magnify any calibration error in the hologram data; thus the microphones in the array must be calibrated so as to have a high relative precision in amplitude and phase. The microphones in the Penn State array were calibrated in situ (using the actual data recording signal paths) using a Bruel and Kjaer microphone coupled to the array microphone with a small leak-tight bellows activated chamber. The calibration data is stored

and used during data acquisition to normalize each hologram data set so that it appears as though it were recorded with the single Bruel and Kjaer microphone, duplicated at each of the 256 array sites. The rather extensive and careful calibration and its test using a theoretically tractable (but non-trivial) source was the project of graduate student Todd Beyer.[26]

With the high-speed data acquisition electronics and computer controlled array transtation system, the Penn State NAH system can record, transform (from the time domain to frequency domain), and calibrate a 64 x 64 point hologram in just a few minutes. In order to match the speed and precision of the data acquisition, fast and efficient computer programs had to be developed for the digital holographic reconstructions. Graduate student Bill Veronesi[20] performed a thorough survey of all the various types of Green's functions, approximations, and computing algorithms in order to determine the best combination for a particular reconstruction. Research associate Yongchun Lee[27] wrote the computer programs which take the maximum advantage of the array processor in all phases of the computations.

For all of the features of the NAH system discussed above (array construction, data acquisition, array calibration and testing, and computer algorithms) comprehensive, detailed papers will be published in the near future.

C. Examples of NAH reconstructions

Figure 5a shows the reconstruction of two point sources, simulated by the low frequency radiation from the ends of two 2.5 cm diameter pipes driven at resonance. The spacing between the ends of the pipes was only 6 cm, whereas the wavelength of the radiation was 3 m. Figure 5b shows the reconstruction of the two point sources using conventional holography which does not include the evanescent waves; the reconstruction shows only a single broad maximum, roughly a wavelength (3 m) in diameter. The NAH reconstruction in Fig. 5a easily pin-points the two sources with a resolution of a few centimeters; with

NAH the resolution is improved by a factor of ~50. One might suppose that reconstructing point sources is easy because of their singular behavior. However, Fig. 5a is a reconstruction of the z-component of the acoustic intensity at the point sources; the intensity of an ideal point source is a product of an infinite pressure amplitude, an infinite velocity amplitude, and the cosine of 90°, giving a finite result. In order to avoid pathological behavior in dealing with large amplitudes and phases close to 90°, the hologram data must be precisely measured, calibrated, and processed. The results in Fig. 5a are a non-trivial test of NAH.

Figure 6 shows a plot of a projection of the vector intensity field in a plane containing the two point sources and perpendicular to the hologram plane. The acoustic energy from the two sources flows together within a distance of only .05 wavelengths.

Figure 7 shows the reconstructed surface velocity of a rectangular plate vibrating in a normal mode which has four nodal lines traversing the width of the plate and two nodal lines traversing the length. By using the vector graphics display, we may observe the actual motion of the plate and visually detect the subtle shifts in phase occurring between the various sections of the plate. For a plate vibrating below coincidence, these phase shifts will have a dramatic effect on the vector intensity pattern above the plate surface.

Figure 8 shows a top view of the vibrating plate of Fig. 7, with different symbols indicating the surface velocity amplitude and approximate relative phase $\Delta\phi$, where $\cos \Delta\phi \approx \pm 1$. The (4,2) nodal line pattern is clearly evident.

Figure 9 shows a plot of the normal component of the acoustic intensity at the surface of the plate of Fig. 7. The interesting features are the regions of negative intensity which cancel the positive intensity regions and greatly

diminish the total radiated power. Figure 10, giving the projected acoustic intensity in a plane through the centerline of the plate and perpendicular to the plane of the plate, shows that the positive and negative intensity regions of the plate are portions of circulating energy flow patterns as discussed in Section II. The circulating energy flow occurs within a fraction of a wavelength of the vibrating plate surface. These circulating patterns are always present for plates vibrating in a normal mode below the coincidence frequency.

Figure 11b shows the holographically reconstructed surface intensity of a plate vibrating in a (2,2) mode; since the plate was below coincidence positive and negative intensity regions are evident. Figure 11a shows the theoretically predicted surface intensity for the (2,2) mode of a plate (with free edges) vibrating in an infinite rigid baffle; the center and edge regions of the baffled plate are quite different from those of the holographically measured plate, which was not baffled. A theoretical calculation of the surface intensity of an unbaffled plate using an iterative computer alogrithm developed by E. G. Williams[28] is shown in Fig 11c; this figure shows good agreement with the experimental result in Fig. 11b. Comparing Fig. 11c with 11a illustrates the significant difference in the surface intensity between a baffled and unbaffled vibrating plate.

Figure 12 is a plot of the surface intensity a plate, thicker than that of Fig. 7-10, which is also vibrating in a (4,2) mode but at a frequency which is above coincidence. In contrast to Fig. 9, the high intensity regions of Fig. 12 are all positive, consistent with the higher radiation efficiency of a plate above coincidence.

Figure 13 shows the intensity field projected onto a plane through the centerline of a rib-stiffened vibrating plate. This plate had a heavy rib bonded across its width as shown by the edge-view of the plate illustrated

in Fig. 13; the rib is located at one-quarter of the length of the plate. The plate is driven at a resonance below coincidence at a point in the center of the plate. The intensity field shows that acoustic energy is transferred to the air at the driver (due to the distortion of the plate by the point force) and near the rib (which also disturbs the bare plate motion so as to lessen cancellation and promote radiation). Figure 14 shows a side view of the same intensity field, projected in the plane containing the rib; the end view of the plate illustrated in Fig. 14 shows the rib extending across the width of the plate. Rather than having a uniform intensity pattern along the rib, the plate has a circulating energy region at the right-hand side. This was a mystery until a close examination of the plate revealed that the epoxy bonding the rib to the plate had come loose along the right-hand section. The circulating flow pattern resulting from the faulty epoxy bond was present at all driving frequencies. It should be noted that the spatial resolution represented in the intensity field plots of Figs. 13 and 14 is considerably smaller than the radiated wavelength. Thus nearfield acoustic holography may be used to pinpoint defects for low frequency non-destructive testing.

V. FURTHER DEVELOPMENTS

A. General

Generalized holography can be a powerful measurement tool when applied to radiation sources or scattering objects which conform to the requirements imposed by a practical data acquisition system. There are numerous types of sources for which the limitations of finite aperture size and dynamic range produce negligible error. There are, of course, sources and environments for which the application of a generalized holography system is impossible or impractical, and other techniques must be used for these sources. However, there are some sources which do not conform to the ideal conditions of generalized holography, but for which the technique may be extended so as to make useful measurements possible. Such sources and environments may occur when generalized holography is used in the field and/or applied to sources or scatters which have a low-symmetry shape, not readily conforming to the level surface of a separable coordinate system. These situations and possible extensions of the technique will be briefly discussed in the next subsections.

B. Development of a field measurement tool

With current technologies, a reasonably-sized microphone array and portable data acquisition electronics may be constructed and used for field measurements of noise sources. Problems which might be encountered in field measurements include:

a) Sources having a physical extent exceeding the size of the array.

b) Reverberent environment

c) Sources having low-symmetry shape

For sources which extend beyond the hologram aperature, it may be possible to make several measurements and combine them in a mosaic. Some assumptions must be made concerning the spatial and temporal coherence of the sources. The mitigating

factor would be that each measurement will be made in the extreme nearfield of the local sources, so that the direct radiation from these sources will dominate each reconstructed field. Once major sources have been quantified, this information can be used as a priori knowledge in artifically extending the aperture of a single hologram. In general, a priori knowledge of the physical configuration of a radiation source may be used to artifically extend the aperture. Computer simulations of this technique are currently in progress.

Field measurements in a reverberent environment may be possible if one has some knowledge of the environmental characteristics. For example, if measurements are made on a source near a rigid wall, then the hologram data might be processed with eigenfunctions $\cos k_z(z-z_{wall})$ rather than $\exp(ik_z z)$. Also a system of images may be used in an iterative or variational processing technique in order to find a field solution consistent with the hologram measurement and the environment. Finally, hologram measurements may be made on two closely spaced parallel surfaces, so that the processing can distinguish between outgoing waves from the source and incoming waves from reflections. This technique has already been successfully employed by G. Weinreich.[22]

Although the discussion above may give the impression that field measurements with holography are difficult, they are no more so than with other techniques. Nearfield holography has the advantage that measurements are made as close to the source as possible, so that the direct field of the source dominate the data. In this case holography provides the fastest, most thorough amount of radiation information available per unit effort.

C. Holography for low-symmetry objects; depth resolution

As discussed in section IV.C, generalized holography can be used to reconstruct the wavefield in a three-dimensional region bounded by the level surface S of a separable coordinate system, where S just touches the physical source. Ideally, one would want the surface of the physical source to coincide with the level surface S, so that generalized holography can be used to reconstruct the normal velocity and intensity directly at the source; in this case a detailed correlation between the properties of the source and the radiated field could be obtained. However, many sources (certainly sources encountered in the field) have shapes which do not conform to level surfaces and which may have important radiating surfaces beyond the level surface S. For example, in plane generalized holography one cannot reconstruct an "image" of the source beyond the plane (parallel to the hologram plane) which just touches the physical source region. It would of course be advantageous to obtain "depth resolution" for holographically reconstructing beyond the surface S.

The reason that generalized holography is restricted to level surfaces of separable coordinate systems is because the Green's functions (for the boundary value problems) are known only for such systems. In order to reconstruct down to the surface of an odd-shaped or low-symmetry source, one must find the Green's function satisfying a homogeneous condition on the source surface. Since in actual implementations of holography the measured and reconstructed fields are discrete and finite, then one may use linear analysis to determine a Green's function matrix. If finite element techniques[29] are combined with the principles of generalized holography, then the size of the matrices and the time required for computations can be significantlly reduced. A hybrid holography/finite-element technique is currently being developed by graduate student Bill Veronesi.[30] An outline of the technique is as follows:

For sound radiation research (as opposed to acoustic imaging) the physical shape of the soruce is assumed known. The surface of the source S′ is divided into a two-dimensional network of finite elements and nodes, as in the conventional technique. Shape functions for both the surface velocity $v(\vec{r}_S,)$ and surface pressure $P(\vec{r}_S,)$ are then constructed using coordinates conforming to the local curvature of the source surface. Linear expansions of the surface velocity and pressure in terms of the shape functions are then inserted into the surface Helmholz integral equation:[31]

$$P(\vec{r}_S,) = \frac{i\mu c}{2\pi k}\iint_{S'} v(\vec{r}_S',)G_0(\vec{r}_S,-\vec{r}_S',)d^2r_S' - \frac{1}{2\pi}\iint_{S'}' P(\vec{r}_S',)\frac{\partial G_0}{\partial n}(\vec{r}_S,-\vec{r}_S',)d^2r_S' \qquad (63)$$

where G_o is the free-space Green's function and the prime on the second integral indicates the principal value. Evaluating the integrals in Equation (63) over the shape functions produces a set of linear equations relating the surface velocity and pressure expansion coefficients.

The next step is to use Green's surface integral to find the pressure at a field point in terms of the surface velocity and pressure:[12]

$$P(\vec{r}) = \frac{1}{4\pi}\iint_{S'}\left[\frac{i\mu c}{k} v(\vec{r}_S,)G_0(\vec{r}-\vec{r}_S,) - P(\vec{r}_S,)\frac{\partial G_0}{\partial n}(\vec{r}-\vec{r}_S,)d^2r_S,\right] \qquad (64)$$

This expression is evaluated at hologram data points, $\vec{r} = \vec{r}_H$, and the integrals are evaluated over the shape functions. Requiring that the resulting expressions for $P(\vec{r}_H)$ least-squares fit the hologram data produces another set of linear equations for the expansion coefficients. The two sets of equations can be solved for the coefficients which then give the source surface velocity and pressure. All other quantities of interest can be calculated from these.

This work is supported by the Office of Naval Research, Physics Division, and the National Aeronautics and Space Administration.

References

1. For a brief review, see for example H. M. Smith, Principles of Holography (Wiley-Interscience, New York, 1969).
2. J. W. Goodman, Introduction to Fourier Optics, (McGraw-Hill, New York, 1968).
3. G. C. Sherman, J. Opt. Soc. Am. 57, 1160 (1967).
4. J. R. Shewell and E. Wolf, J. Opt. Soc. Am. 58, 1596 (1968).
5. E. Lalor, J. of Math. Physics 9, 2001 (1968).
6. H. G. Schmidt-Weinmar, in Inverse Source Problems, ed. H. P. Baltes (Springer-Verlag, Berlin, 1978) p. 83.
7. J. D. Maynard and E. G. Williams, Proc. NOISE-CON 81, ed. L. H. Royster, F. D. Hart, and N. D. Stewart (Noise Control Foundation, New York, 1981) p. 19-24.
8. M. C. Junger and D. Feit, Sound, Structures, and their Interaction (MIT Press, Cambridge, 1972).
9. A. D. Pierce, Acoustics, an Introduction to its Physical Principles and Applications, (McGraw-Hill, New York, 1981).
10. F. J. Fahy, J. Acoust. Soc. Am. 62, 1057 (1977); J. Chung and J. Pope, GM Research Lab, GMR-2645 (1978).
11. F. T. S. Yu, Introduction to Diffraction, Information Processing, and Holography, (MIT Press, Cambridge, 1973).
12. P. M. Morse and H. Feshbach, Methods of Theoretical Physics, (McGraw-Hill, New York, 1953) Vol. I, p. 803-833.
13. J. S. Bendat and A. G. Piersol, Measurement and Analysis of Random Data, (Wiley, New York, 1966).
14. A. V. Oppenheim and R. W. Schafer, Digital Siganl Processing, (Prentice Hall, Englewood Clifts, NJ, 1975).
15. See, for example, Acoustical Holography, Vol. 1-7 (Plenum, New York, 1967-1976).
16. Lord Rayleigh, Phil. Mag 43, 259 (1897).

17. R. N. Bracewell, The Fourier Transform and its Applications, (McGraw-Hill, New York, 1978) p. 143.

18. M. Born and E. Wolf, Principles of Optics (Oxford, 1965) p. 563.

19. J. Powers, in Acoustical Holography, ed. L. W. Kessler (Plenum, New York, 1976) Vol. 7, p. 193; D. L. Van Rooy, IBM Publications No. 320.2402, Houston Scientific Center, 1971.

20. W. A. Veronesi and J. D. Maynard, J. Acoust. Soc. Am. 75, S71 (1984).

21. Y. Huang, W. A. Veronesi, and J. D. Maynard, J. Acoust. Soc. Am. 75, S71 (1984).

22. G. Weinreich and E. B. Arnold, J. Acoust. Soc. Am. 68, 404 (1980).

23. P. R. Stepanishen and K. C. Benjamin, J. Acoust. Soc. Am. 71, 803 (1982); P. Stephanishen and H. W Chen, J. Acoust. Soc. Am. 74, S24 (1983).

24. J. D. Maynard, J. Acoust. Soc. Am. 74, S37 (1983).

25. D. J. Bowen and J. D. Maynard, J. Acoust. Soc. Am. 75, S71 (1984).

26. T. D. Beyer, Test of the Nearfield Acoustical Holography Technique Using an Unbaffled, Uniformly Oscillating Disk, Ph.D. Thesis, The Pennsylvania State University, 1984.

27. Y. Lee and J. D. Maynard, J. Acoust. Soc. Am. 75, S71 (1984).

28. E. G. Williams, J. Acoust. Soc. Am. 74, 343 (1983).

29. O. C. Zienkiewicz, The Finite Element Method, (McGraw-Hill, London, 1977).

30. W. A. Veronesi and J. D. Maynard, J. Acoust. Soc. Am. 75, S71 (1984).

31. R. Courant and D. Hilbert, Methods of Mathematical Physics, (Interscience, New York, 1962) Vol. II, p. 526.

FIGURE CAPTIONS

Fig. 1. Schematic representation of the holographic reconstruction process, illustrating propagating and evanescent waves.

Fig. 2. The wrap-around problem. a) Periodic repetition of the source caused by its representation by a discrete Fourier series. b) The Green's function to be convolved with the source. c) The source with a guard-band of zeroes. d) The truncated Green's function.

Fig. 3. Zoom imaging. a) The finite hologram aperture may result in only a few data points falling within the radiation circle. b) For calculation of farfield quantities, a higher density of data points may be mapped into the radiation circle.

Fig. 4. The Penn State Nearfield acoustic Holography system for airborne sound radiation research. Illustrated are the 256 microphone array, the data acquisition electronics, and the data processing and display equipment.

Fig. 5. Holographic reconstruction of the intensity of two point sources. a) Nearfield holography. b) Conventional holography.

Fig. 6. Acoustic intensity vector field from two point sources.

Fig. 7. Nearfield Acoustic Holography reconstruction of the surface velocity of a rectangular plate vibrating in a (4,2) mode.

Fig. 8. Top view of the plate in Fig. 7. The different symbols indicate approximate amplitude and phase.

Fig. 9. Normal component of the acoustic intensity at the surface of the plate of Fig. 7.

Fig. 10. Projected acoustic intensity in a plane through the center line of the plate of Fig. 7.

Fig. 11. Surface intensity of a plate vibrating in a (2,2) mode. a) Theoretical unbaffled plate. b) Experimental result from Nearfield Acoustic Holography (unbaffled plate). c) Theoretical baffled plate.

Fig. 12. Surface intensity of a thick plate vibrating in a (4,2) mode above coincidence.

Fig. 13. Acoustic intensity in a plane through the centerline of a center-driven, rib-stiffened plate.

Fig. 14. Acoustic intensity in a plane through the rib of the plate of Fig. 13. The circulating energy flow pattern locates faulty bonding of the rib.

WAVELENGTH $\lambda = \frac{2\pi c}{\omega}$

(x, y) - FT → (k_x, k_y)

$$k_z = \sqrt{\left|\left(\frac{2\pi}{\lambda}\right)^2 - (k_x^2 + k_y^2)\right|}$$

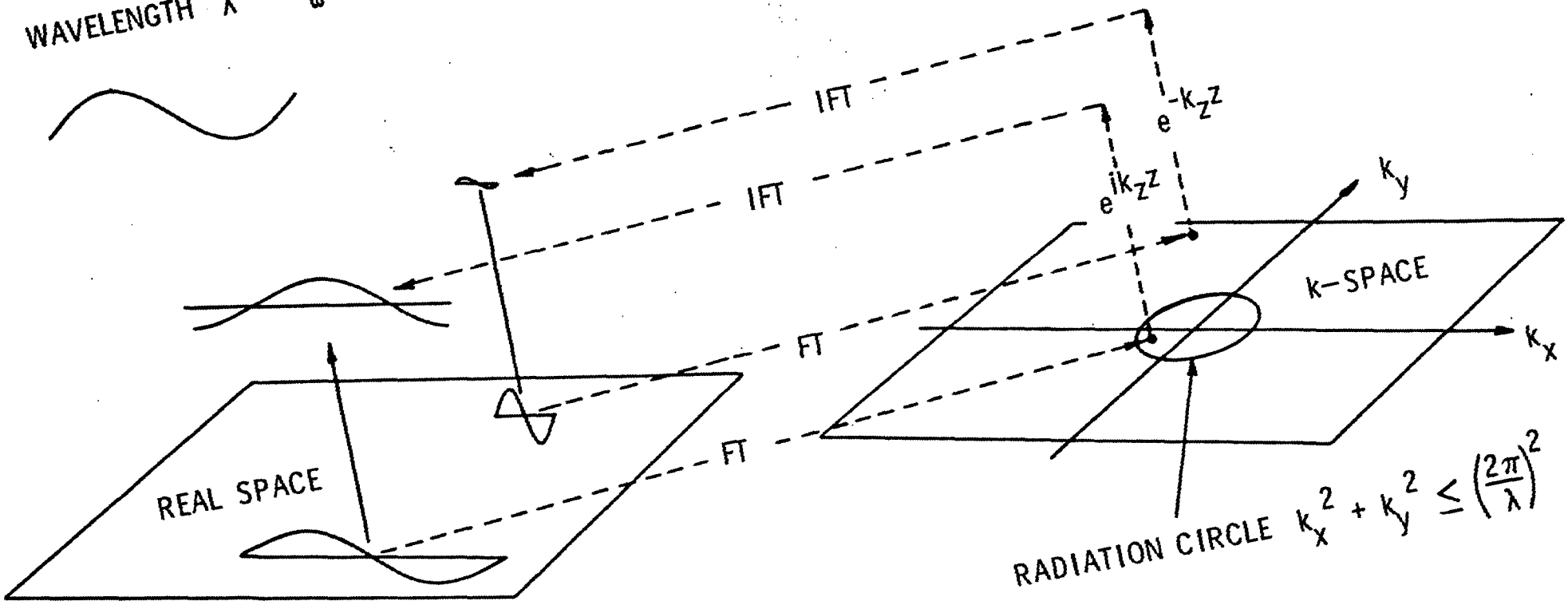

Figure

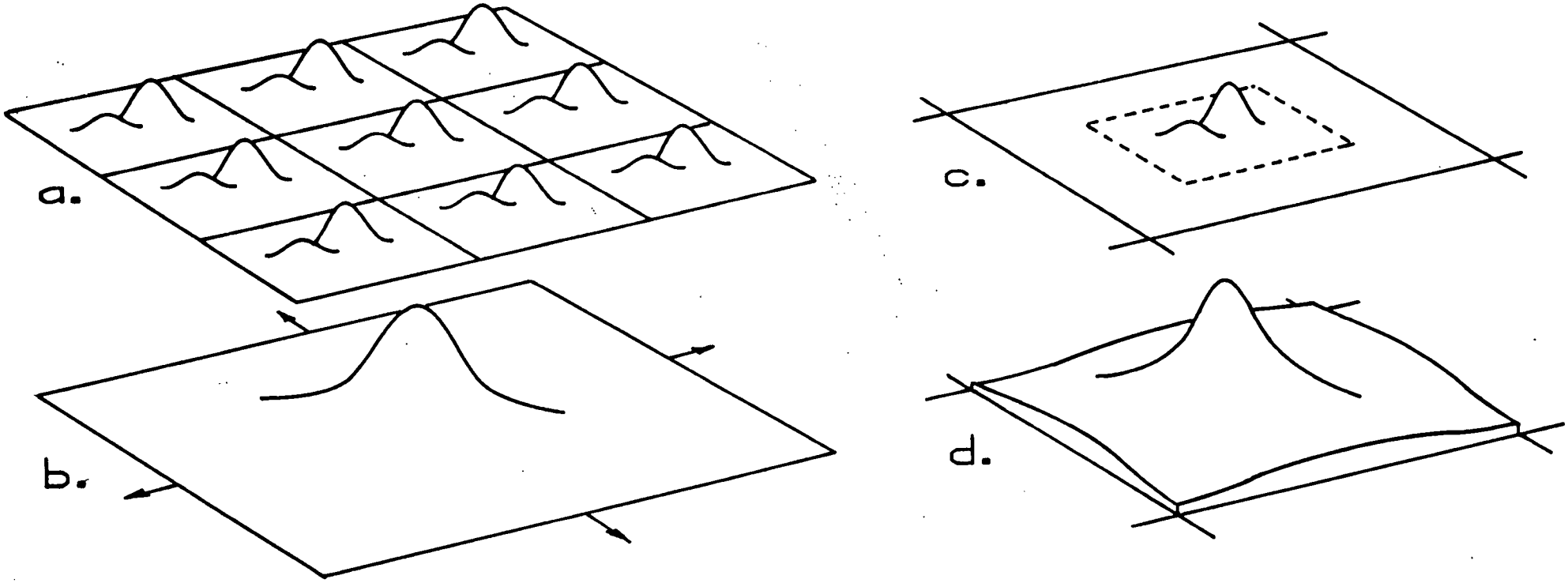

Figure 2

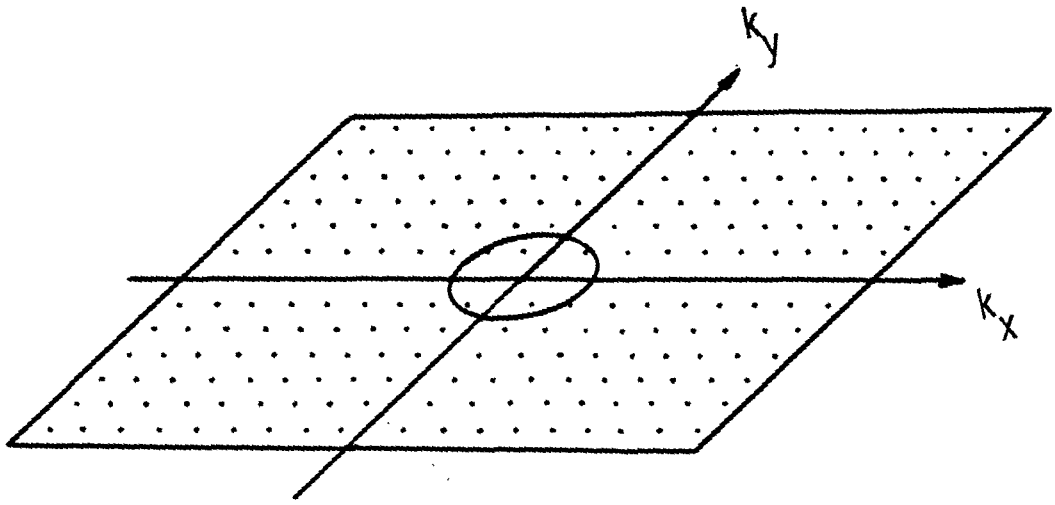

a.

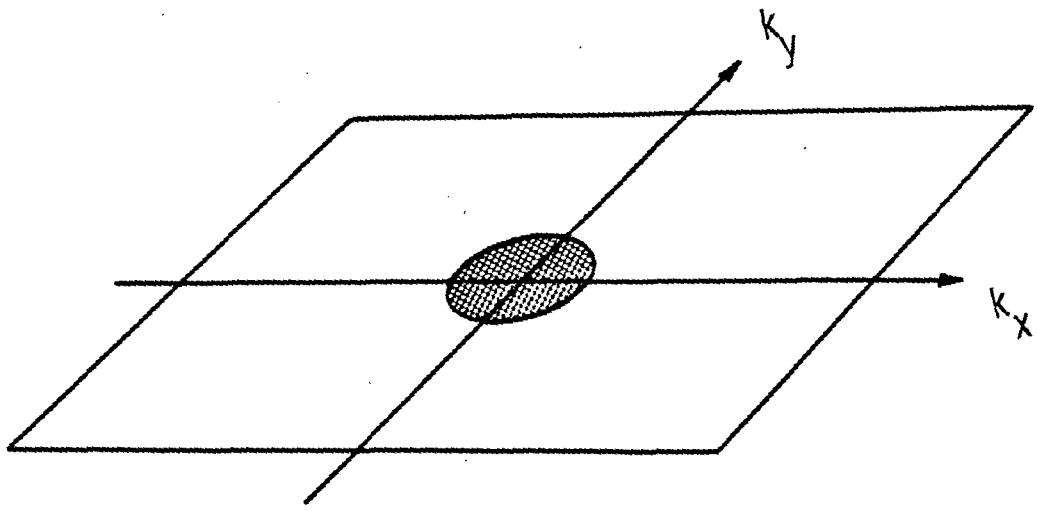

b.

Figur

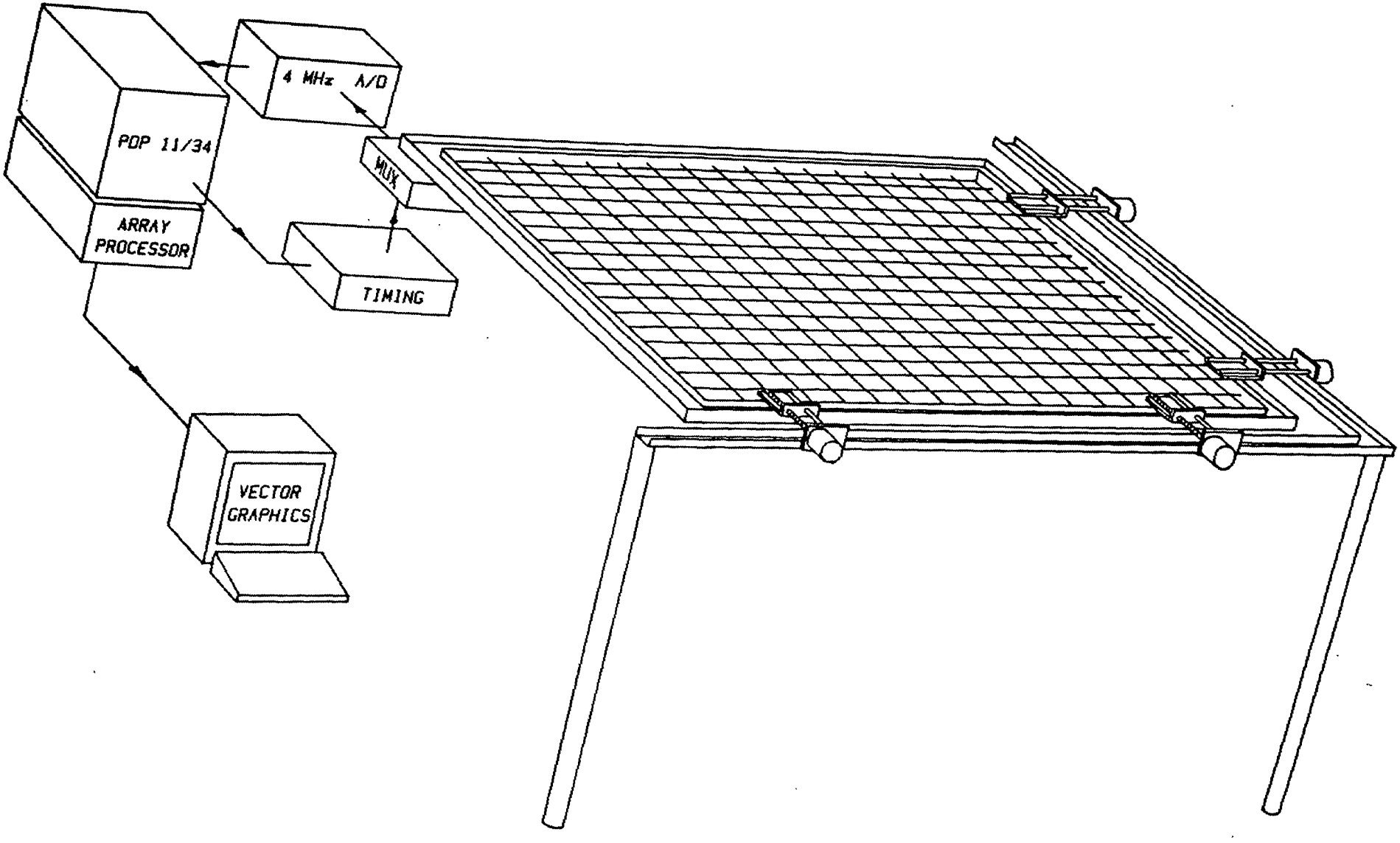
4 MHz A/D
PDP 11/34
ARRAY PROCESSOR
MUX
TIMING
VECTOR GRAPHICS

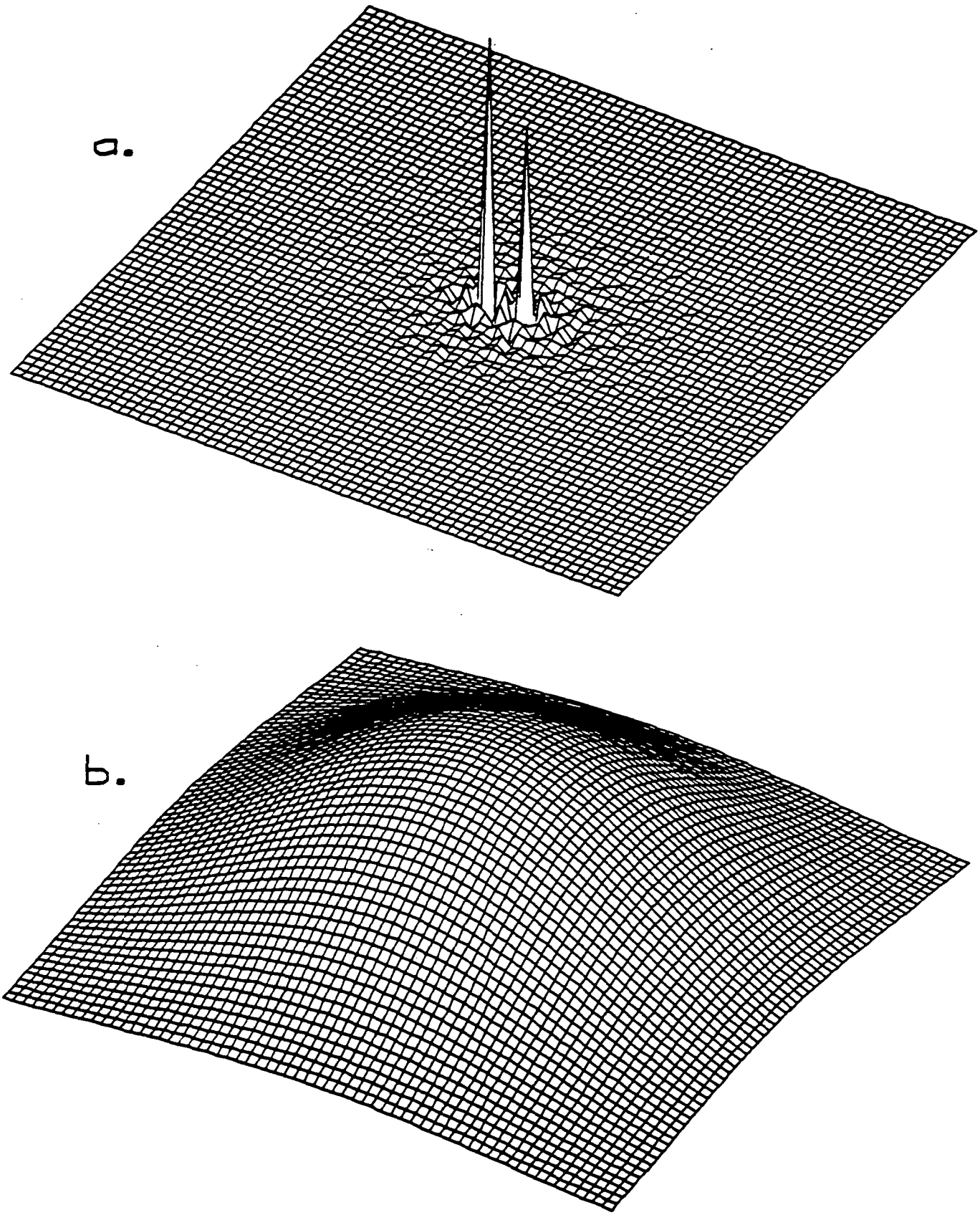

Figure 5

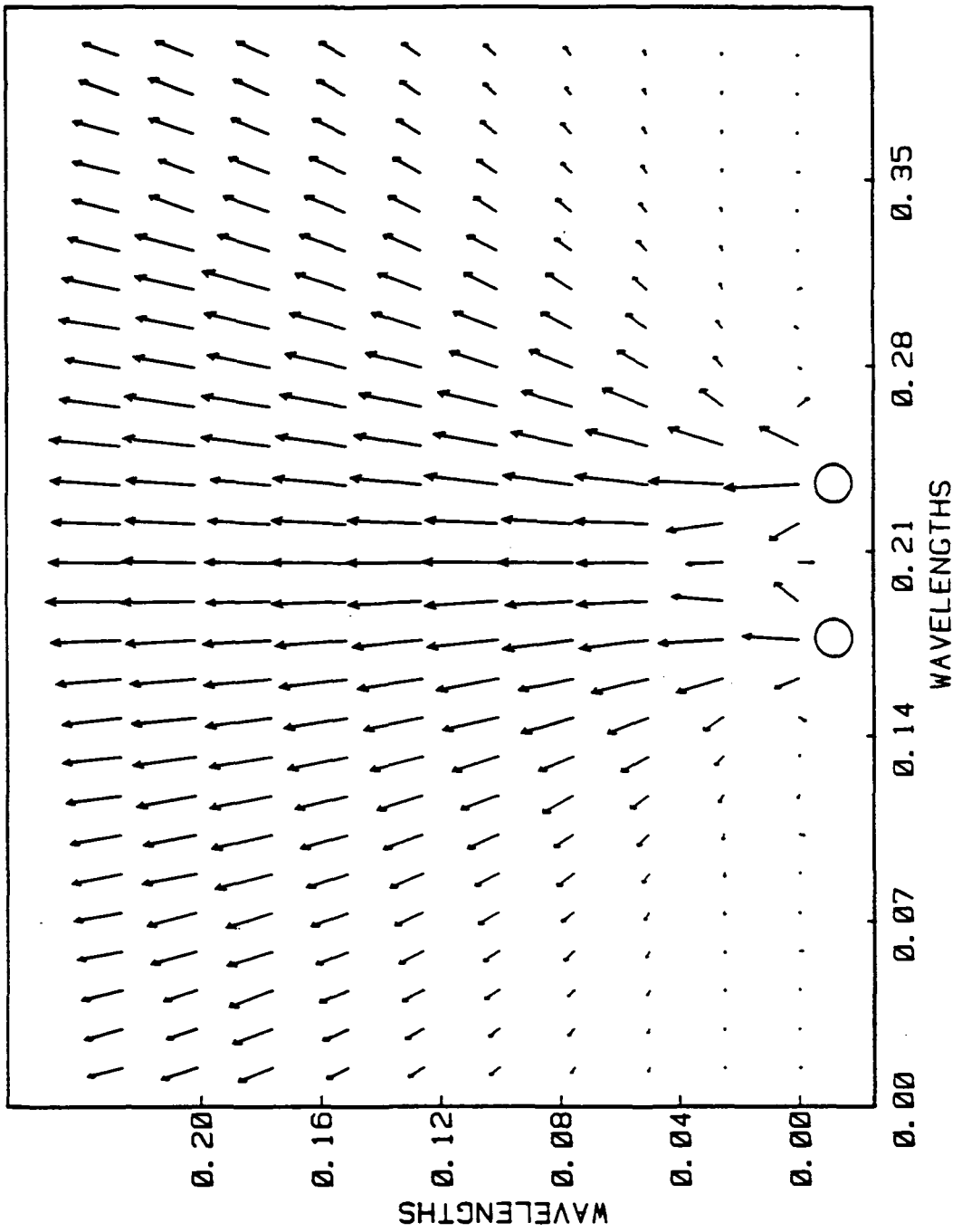
0.20
0.16
0.12
0.08
0.04
0.00
WAVELENGTHS
0.00
0.07
0.14
0.21
0.28
0.35
WAVELENGTHS

Figure 6

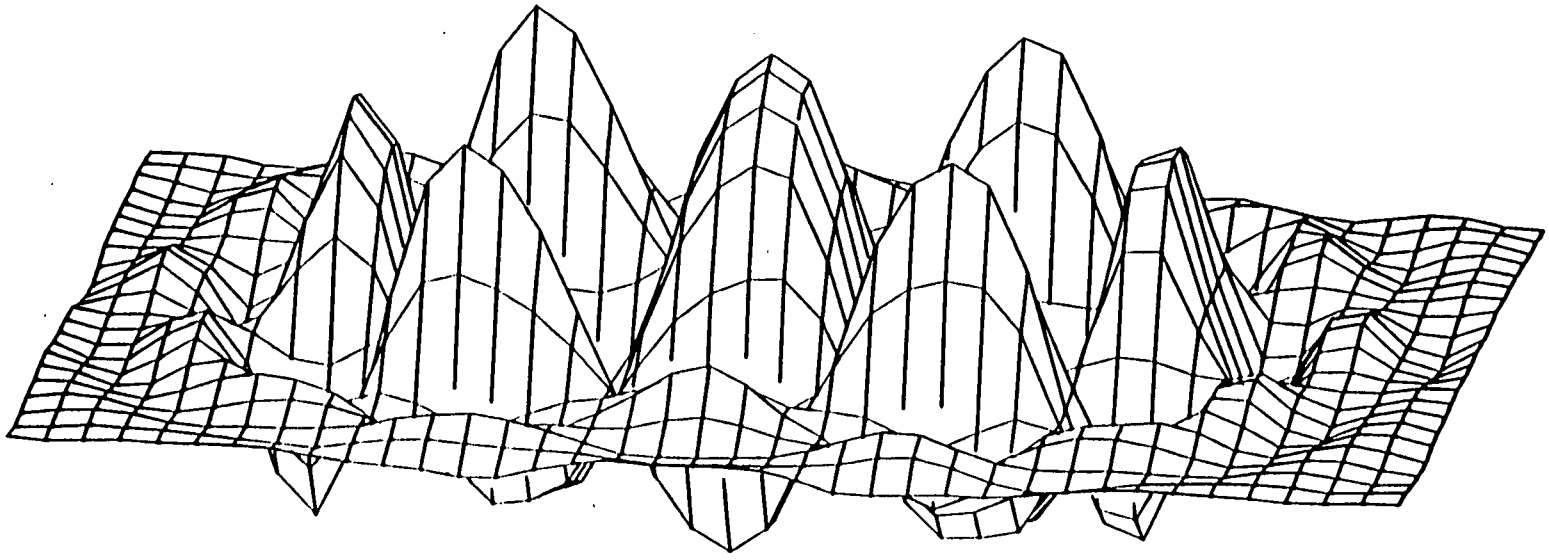

Figure 7

Figure 8

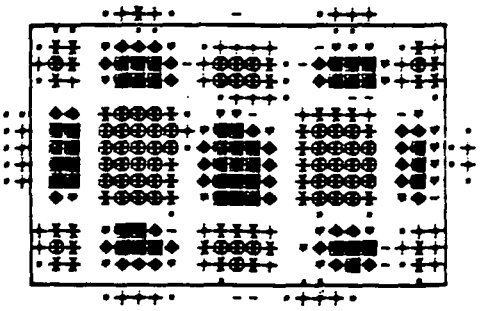

POS		NEG
●	0- 4	■
*	4- 8	◆
+	8-12	•
·	12-16	-

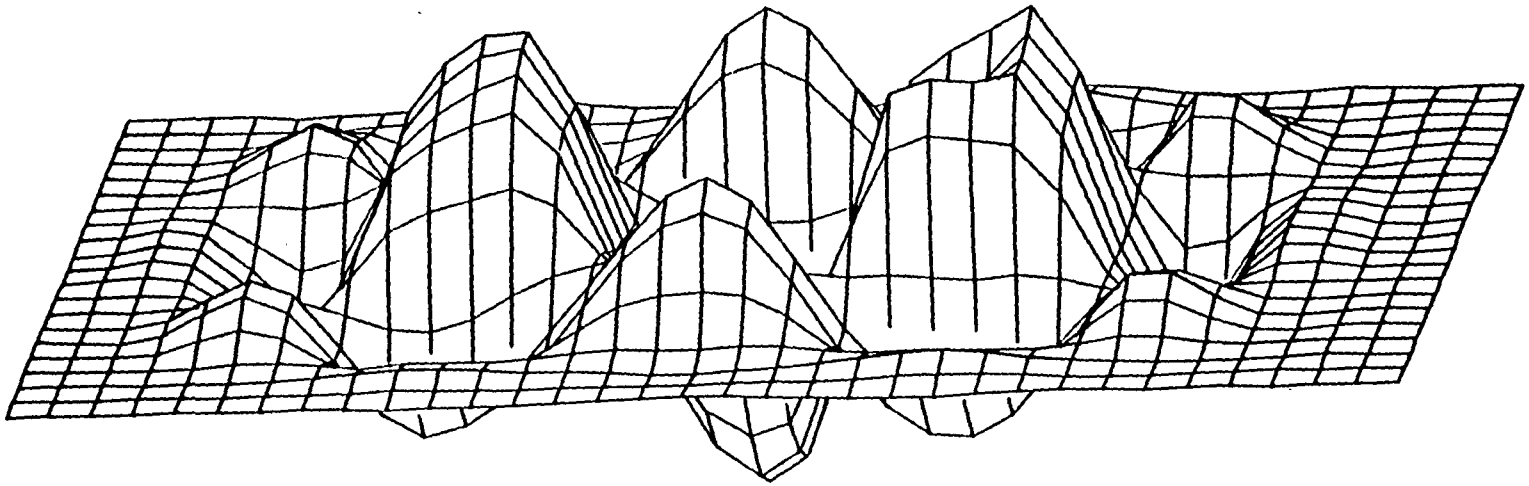

Figure 9

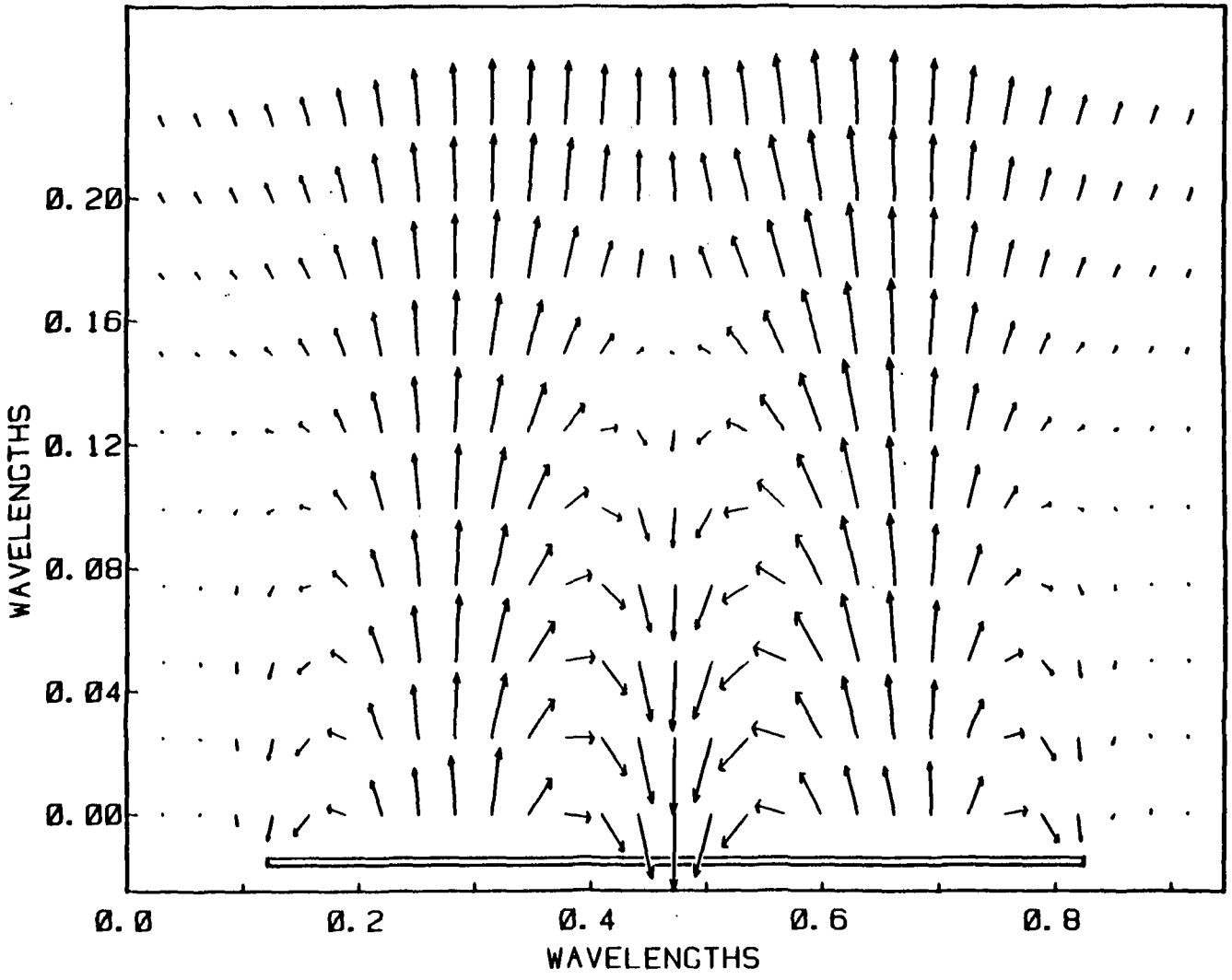
0.20
0.16
0.12
0.08
0.04
0.00
WAVELENGTHS
0.0
0.2
0.4
0.6
0.8
WAVELENGTHS

Figure 10

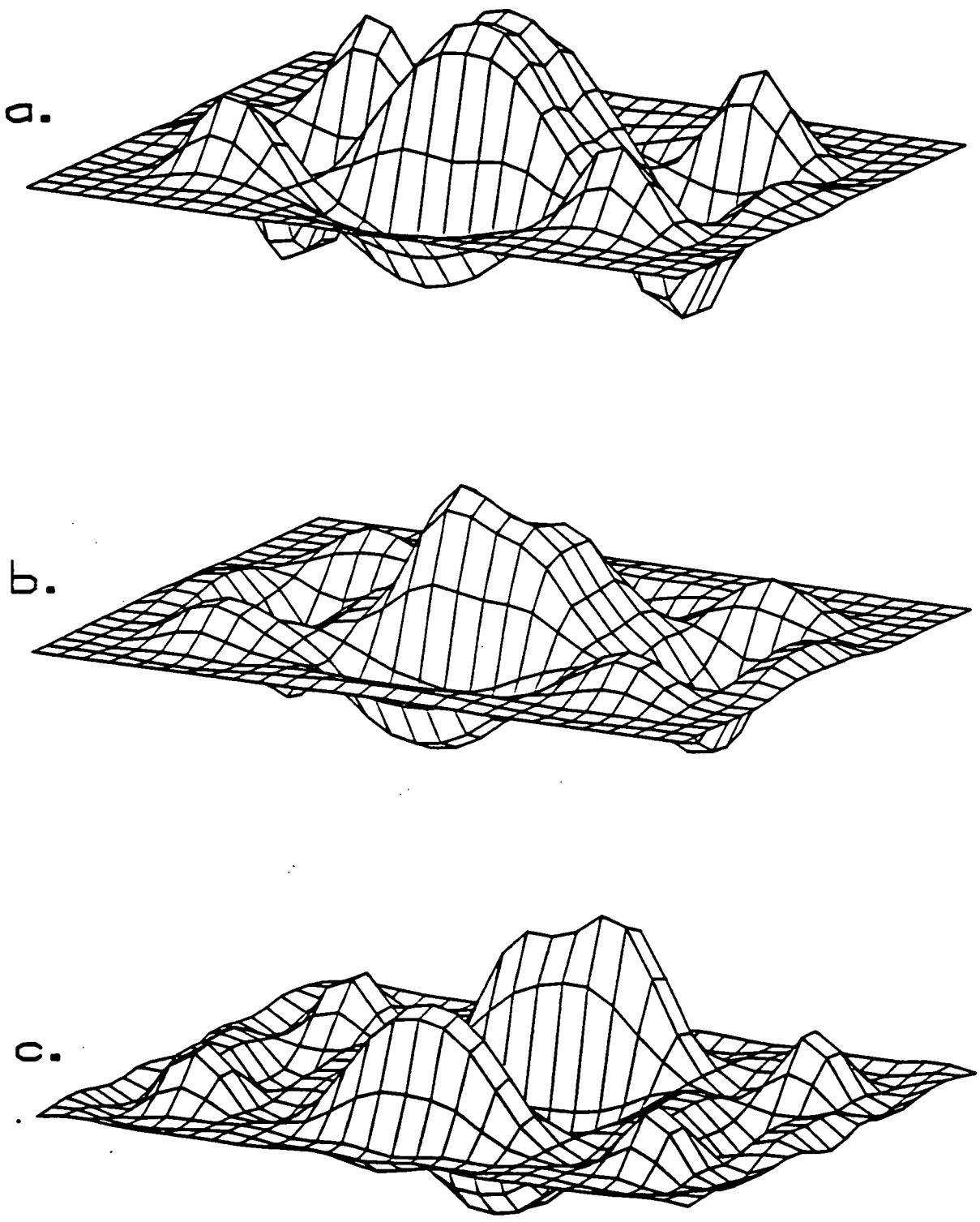

Figure 11

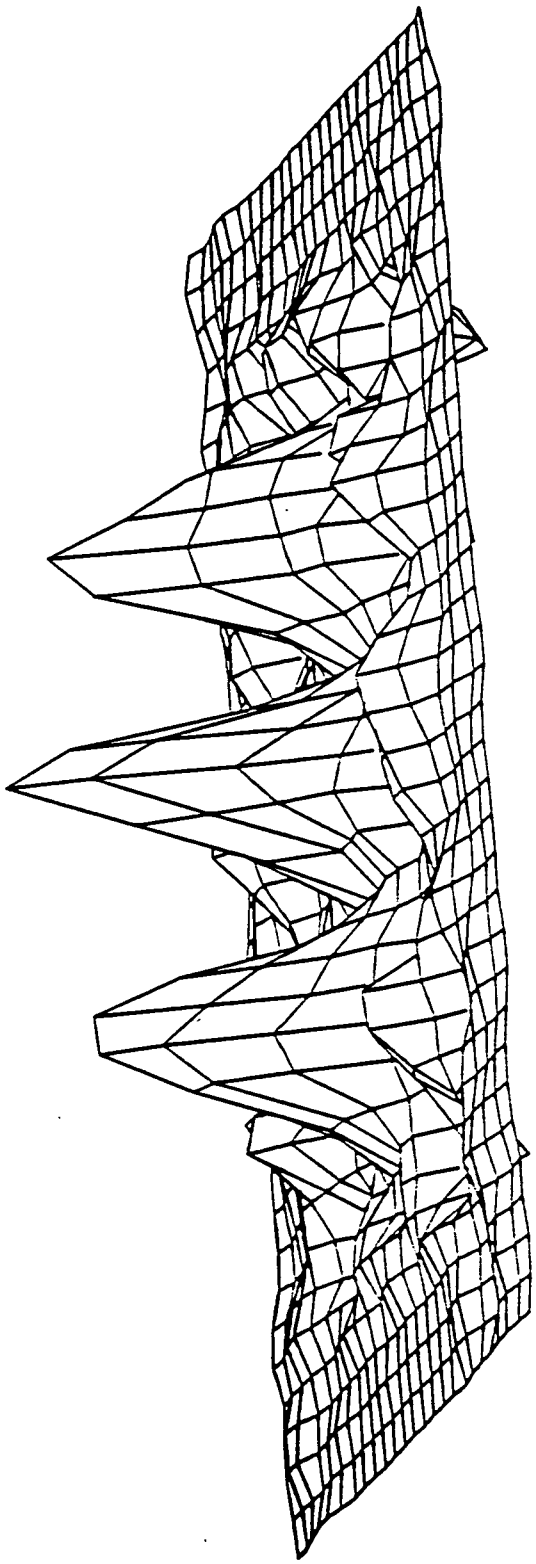

Figure 12

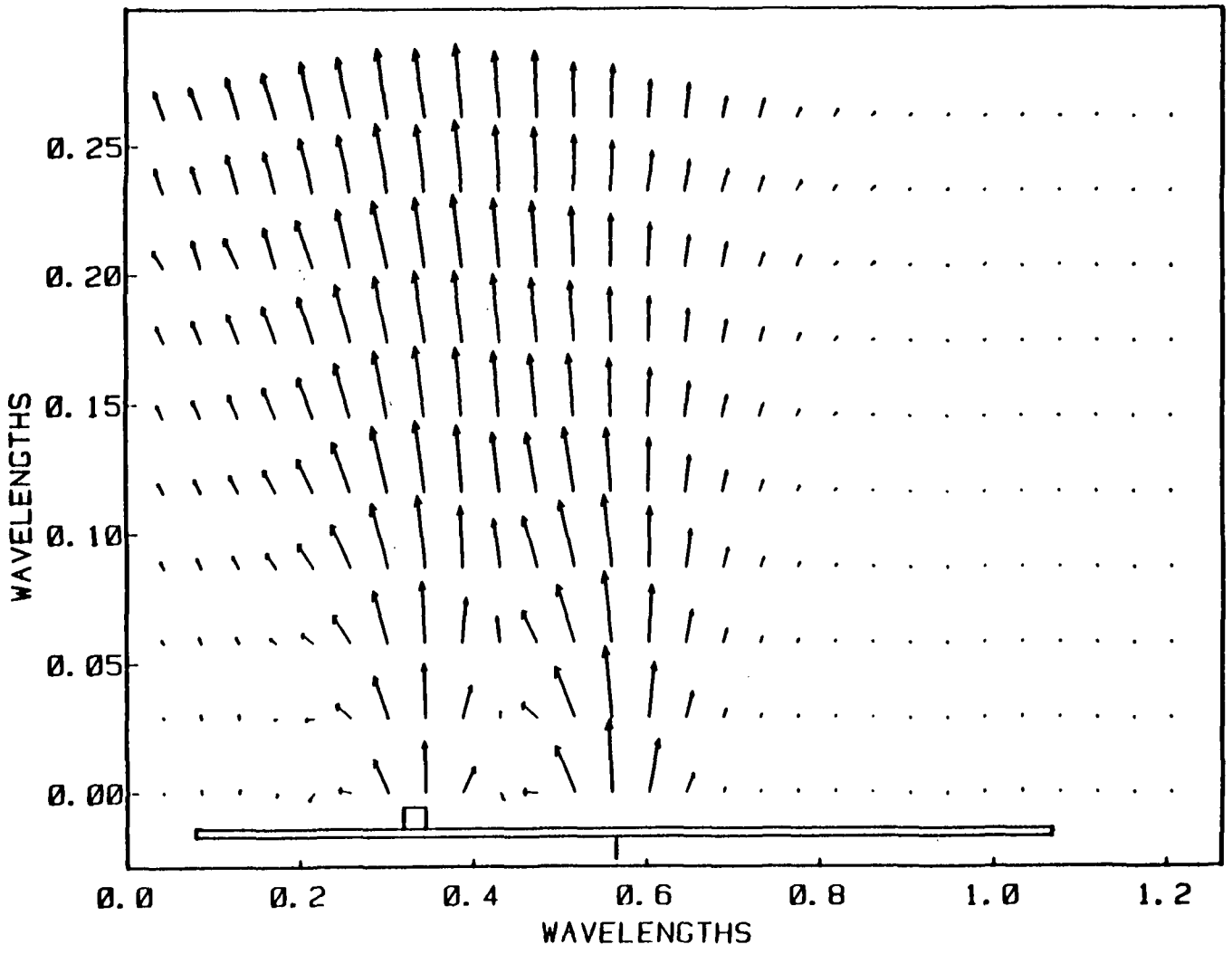
0.25
0.20
0.15
0.10
0.05
0.00
WAVELENGTHS
0.0
0.2
0.4
0.6
0.8
1.0
1.2
WAVELENGTHS

Figure 13

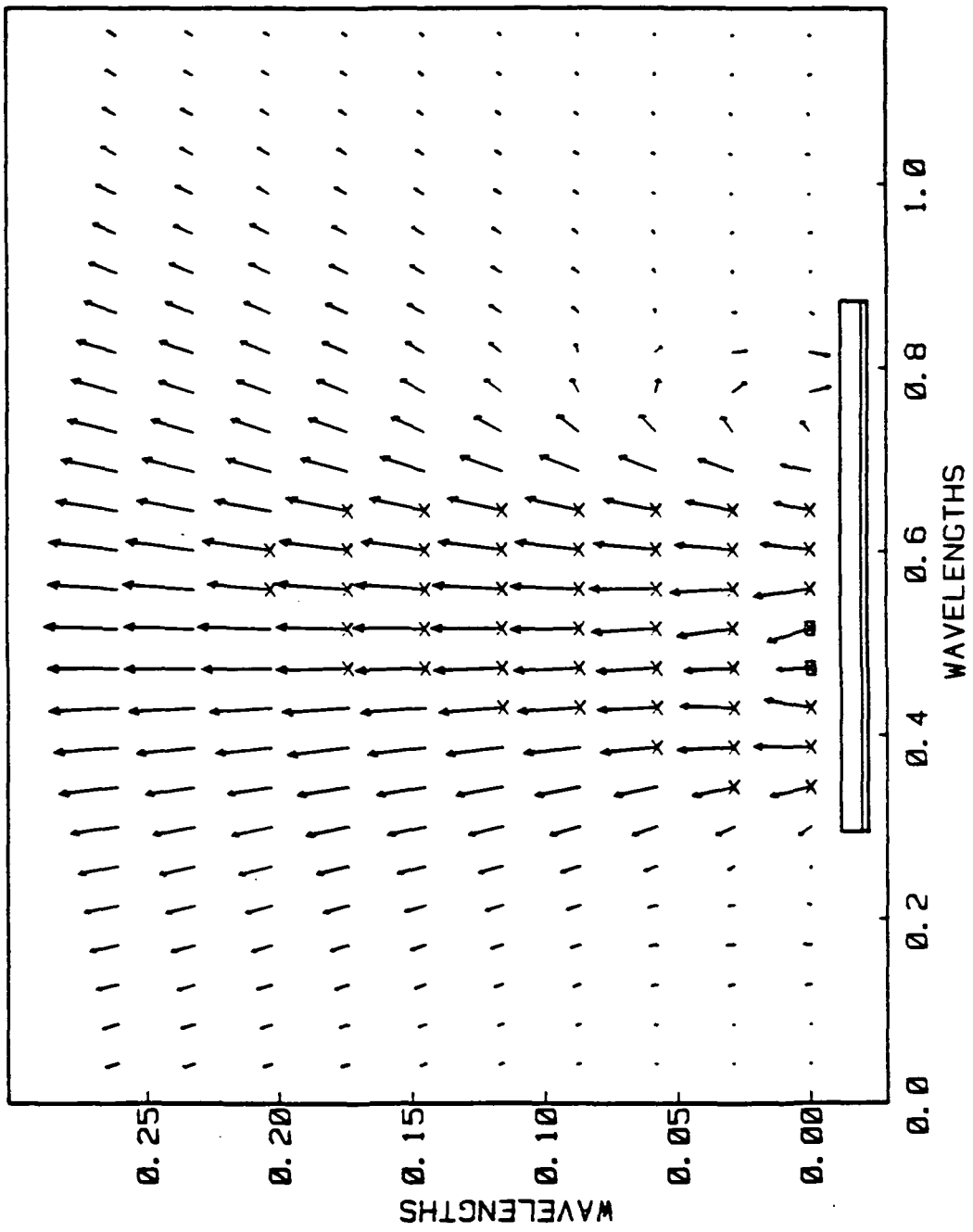
0.25
0.20
0.15
0.10
0.05
0.00
WAVELENGTHS
0.0
0.2
0.4
0.6
0.8
1.0
WAVELENGTHS

Figure 14

APPENDIX II

Advances in Nearfield Acoustical Holography (NAH) algorithms I. Green's functions. William A. Veronesi and J. D. Maynard (Department of Physics and the Applied Research Laboratory, The Pennsylvania State University, University Park, PA 16802)

For efficiency, the spatial proccesing algorithms of NAH, based on Rayleigh's Integrals, utilize the Fast Fourier Transform (FFT). In NAH, the FFT has been treated as an approximation to the continuous Fourier Transform, and with this view, work has been done to reduce the errors introduced by the finite and discrete FFT. In this paper, it is shown that, by using the exact discrete convolution capabilities of the FFT and Inverse FFT, as opposed to its approximate correspondence to the continuous Fourier Transform, algorithms yielding more accurate results are obtained. The essential step is to replace the continuous field over the surface from wich the data was gathered with a piece-wise constant field, each patch having the constant field value as at a contained, measured point. With the field so replaced, Rayleigh's Integral is reduced to a finite, discrete convolution of the measured data with the integrals of the kernel, or Green's function, over each patch. Most importantly, this process totally eliminates the effects of image sources. Conditions for validity of this model are presented, and results for a baffled piston source demonstrate the accuracy of this approach. [Work supported by ONR and NASA]

Technical committee: Physical Acoustics
Subject Classification numbers: 43.20.Rz,43.60.Gk
Telephone number: (814) 865-7841
Send acceptance or rejection notice to:
W. A. Veronesi
104 Davey Lab Box 86
University Park, PA. 16802

Advances in Nearfield Acoustical Holography (NAH) algorithms II: Zoom imaging. Yanmin Huang, William A. Veronesi, and J. D. Maynard (Department of Physics and the Applied Research Laboratory, The Pennsylvania State University, University Park, PA 16802)

In NAH, it is often desireable to increase the density of points in the transform space beyond the density produced by a simple 2-D discrete Fourier Transform of the input data array. Two equivalent methods of increasing the density of points are presented. The two methods are: augmenting the original data with zeroes before transforming, or convolving the transform of the unaugmented data array with the transform of a two dimensional square unit step function. Augmenting with zeroes and the equivalent convolution approach are based on the assumption that surface. Although the hologram and its transform are two-dimensional, the density increasing schemes can be cast in a one dimension at a time form resulting in a great reduction in computation time. This technique has great utility when restricted to increasing the density of points inside the Radiation Circle . When the Radiation Circle originally contains relatively few points, the direct convolution is faster, also this method is not limited to power of two increases in density. Results for propagating the pressure field from a baffled piston source are given. [Work supported by ONR and NASA]

Technical committee: Physical Acoustics
Subject Classification numbers: 43.20.Rz,43.60.Gk
Telephone number: (814) 865-7841
Send acceptance or rejection notice to:
W. A. Veronesi
104 Davey Lab Box 86
University Park, PA. 16802

The Implementation of Nearfield Acoustic Holography with an Array Processor. Yongchun Lee and J.D. Maynard (Dept. of Physics and Applied Research Laboratory, The Pennsylvania State University, University Park, PA 16802)

The data reduction capabilities of our Nearfield Acoustic Holography (NAH) system have been greatly enhanced through the development of efficient computer algorithms utilizing an array processor with a minicomputer. The array processor accelerates not only the FFT computation, but also the Green's function calculation, data windowing, graphics display generation, and zoom imaging. In this paper, the various technigue, which have reduced the NAH processing time by a factor of ~20, will be discussed. This new processing system speeds data collection and processing and will permit measurement of radiation from wideband noise sources with a large number of frequency components.

[Work supported by ONR and NASA.]

Technical committee: Physical Acoustics
Subject Classification number(s): 43.85.Dj, 43.60.Gk
Telephone number: (814) 865-7041
Send acceptance or rejection notice to Yongchun Lee

Experimental Studies of Acoustic Radiation for Unbaffled Complex Planar Sources with Nearfield Acoustic Holography. Yongchun Lee and J.D. Maynard (Dept. of Physics and Applied Research Laboratory, The Pennsylvania State University, University Park, PA 16802)

Design data for the evaluation of the acoustic radiation coupling loss factor for complex planar sources, such as ribbed plates, nonuniform plates, damped plates and aircraft panels etc. is still fairly scarce. This work presents a broad survey of complex vibrating planar sources. These results were obtained using Nearfield Acoustic Holography (NAH) to illuminate the effects of stiffness, mass and damping on radiation loss factor.

[Work supported by ONR and NASA.]

Technical committee: Physical Acoustics

Subject Classification numbers: 43.20.Rz, 43.55.Rg, 43.85.Dj

Telephone number: (814) 865-7841

Send acceptance or rejection notice to Yongchun Lee

Nearfield Holography for wideband sources. Donald J. Bowen and J.D. Maynard (Dept. of Physics and Applied Research Laboratory, The Pennsylvania State University, University Park, PA 16802)

Nearfield Acoustical Holography (NAH), a process developed at the Pennsylvania State University, has proved itself to be a powerful research tool in the study of single-frequency sound sources. A new high-speed data aquisition system has been developed which permits extension of the Nearfield Acoustical Holography technique to the study of wideband noise sources. Using a partially-parallel, partially-sequential sampling network, near simultaneous sampling is achieved for 256 microphones in the holographic measurement plane, for acoustic frequencies up to 1500 Hz. Special problems encountered during the development of the high-speed data aquisition system are discussed.

[Work supported by ONR and NASA.]

Technical committee: Physical Acoustics

Subject Classification number(s): 43.50.Yw, 43.85.Dj, 43.60.Gk

Telephone number: (814) 865-7841

Send acceptance or rejection notice to D.J. Bowen

Special facility: none

Holographic reconstruction of odd-shaped 3-D sources. William A. Veronesi and J. D. Maynard (Department of Physics and the Applied Research Laboratory, The Pennsylvania State University, University Park, PA 16802)

As previously described, [J. D. Maynard , J. Acoust. Soc. Am. 74, S37 (1983)], Nearfield Acoustical Holography can reconstruct the surface velocity and pressure over a level surface in a separable coordinate system from measurements of the radiated pressure field over a parallel level surface. This study investigates the feasability of reconstructing the surface pressure and normal velocity over surfaces wich do not conform to a level surface. Such a reconstruction involves numerically determining a distribution of surface pressure and velocity which satisfies the Surface Helmholtz Integral Equation and which is consistent with the Helmholtz Integral Equation for the pressure field measured on the level surface. Details of the algorithm and results of computer simulations for a uniformly pulsating sphere and a piston set in a sphere (measurements simulated over a planar surface) are presented. [Work supported by ONR and NASA]

Technical committee: Physical Acoustics
Subject Classification numbers: 43.20.Rz,43.60.Ck
Telephone number: (814) 865-7941
Send acceptance or rejection notice to:
W. A. Veronesi
104 Davey Lab Box 96
University Park, PA. 16802